UNIVERSITY OF OKLAHOMA

GRADUATE COLLEGE

THE PACIFIC DECADAL PRECESSION AND ITS RELATIONSHIP TO

TROPICAL PACIFIC DECADAL VARIABILITY IN CMIP6 MODELS

A THESIS

SUBMITTED TO THE GRADUATE FACULTY

in partial fulfillment of the requirements for the

Degree of

MASTER OF SCIENCE IN METEOROLOGY

By

MATTHEW H. ROGERS
Norman, Oklahoma
2020

THE PACIFIC DECADAL PRECESSION AND ITS RELATIONSHIP TO
TROPICAL PACIFIC DECADAL VARIABILITY IN CMIP6 MODELS

A THESIS APPROVED FOR THE
SCHOOL OF METEOROLOGY

BY THE COMMITTEE CONSISTING OF

Dr. Jason C. Furtado, Chair

Dr. Naoko Sakaeda

Dr. Elinor R. Martin

Acknowledgments

I would like to acknowledge the committee members Dr. Elinor Martin and Dr. Naoko Sakaeda for their feedback and assistance in both the classroom and during the process of finishing this thesis. I would also like to extend my gratitude to my committee chair, Dr. Jason Furtado, for his unparalleled patience and commitment to both listening and instructing. I could not have asked for a better mentor. Though they were not directly influencing the content within this thesis, I would like to thank both friends and family for their continual support over the last several years. Without them the following pages would contain nothing more than white space. Finally, I acknowledge the World Climate Research Programme, which, through its Working Group on Coupled Modelling, coordinated and promoted CMIP6. I thank the climate modeling groups for producing and making available their model output, the Earth System Grid Federation (ESGF) for archiving the data and providing access, and the multiple funding agencies who support CMIP6 and ESGF.

Table of Contents

List of Tables

List of Figures

Abstract

Persistent, multi-year shifts in atmospheric circulations and their associated influence on regional climates can have profound impacts on physical, biological, and socioeconomic systems. The Pacific Decadal Precession (PDP), a quasi-decadal mode of variability in the North Pacific, describes a series of such shifts in atmospheric circulations. Unlike previously established modes of quasi-decadal variability, the PDP is characterized by the cyclonic progression of an atmospheric pressure anomaly dipole around the North Pacific and has been connected to climate variations across North America. The north-south (N-S) oriented phase of the PDP (i.e., when the pressure dipole is oriented meridionally) has been hypothesized to be partially driven by decadal variability in central Pacific (CP) sea surface temperatures given its similarities to the North Pacific Oscillation (NPO). This thesis investigates this hypothesis by identifying connections between the N-S phase of the PDP, the NPO, and tropical Pacific decadal variability (PDV), in both reanalysis and select models from the Coupled Model Intercomparison Project phase 6 (CMIP6) archive. The analyses here show that the N-S phase of the PDP is indeed related to the NPO, as the quasi-decadal temporal evolution of the NPO tracks the PDP well. However, there is a considerable portion of variability in the PDP that is not explained by the NPO which is likely due to the NPO not explaining variability associated with the east-west orientation of the PDP. This thesis also shows that the emergence of the N-S phase is both related to and influenced by tropical Pacific decadal sea surface temperature variability, specifically variability associated with CP El Niño-Southern Oscillation (ENSO) events. The link between the N-S phase of the PDP and CP ENSO events is demonstrated by the similarity in sea surface temperature anomaly patterns associated with both the emergence of the N-S phase of the PDP and the structure of CP ENSO events, and highly significant temporal correlations between the two patterns. In contrast to reanalysis, current climate models struggle with simulating the evolution of the

PDP, and in general do not capture the observed relationships between the PDP, the NPO, and tropical PDV. Potential reasons for models not capturing the relationships between the PDP, NPO, and tropical PDV are discussed briefly to motivate future research. While this thesis finds evidence supporting connections between the PDP and other modes of Pacific variability, more understanding of the dynamics of the PDP and how current models simulate it is needed. Establishing a better understanding of the dynamics of the PDP and further assessment of these dynamics in models will aid in improving current prediction capabilities of the PDP and PDP-related regional climate impacts.

Chapter 1

Introduction

Large-scale climate variations, like the North Pacific Gyre Oscillation (NPGO) (Di Lorenzo et al., 2008), the North Pacific Oscillation (NPO) (Rogers, 1981), and the Pacific Decadal Oscillation (PDO) (Mantua et al., 1997), have been linked to significant regional climate shifts in the North Pacific. Examples of such shifts include persistent drought in California (Diffenbaugh et al., 2015), anomalously warm sea surface temperatures (SSTs) in the Gulf of Alaska (Bond et al., 2015; Di Lorenzo and Mantua, 2016), and the disruption of marine ecosystems in the Pacific (Mantua et al., 1997; Di Lorenzo et al., 2008). The severity of these impacts has motivated considerable research focused on the dynamics of these modes of variability and their impacts (Rogers, 1981; Mantua et al., 1997; Newman et al., 2003; Duffy et al., 2005; Schneider and Cornuelle, 2005; Di Lorenzo et al., 2008, 2010). Understanding the dynamics of climate variability in the Pacific has proven difficult, as the interactions between various modes of variability in both the tropics and extratropics are complex (Pierce et al., 2001; Deser et al., 2017; Zhang et al., 2018b; Capotondi et al., 2018; Sun and Okumura, 2019). Still, efforts to isolate the contributions of each mode of variability and how they feedback onto each other have proved to be valuable in improving forecasts both globally and regionally (Goddard and Dilley, 2005; Zhang, 2005). Advances made in our understanding of natural variability in the Pacific is useful in mitigating physical, biological, and economic impacts from regional climate shifts, and will prove to be even more important in understanding how natural variability will evolve under future climate change.

1.1 Pacific Variability: Background

Perhaps the most influential and researched phenomena in the Pacific basin is the El Niño-Southern Oscillation (ENSO), a coupled atmosphere-ocean mode of interannual variability characterized by a periodic warming and cooling of the eastern equatorial Pacific coinciding with a see-saw in sea level pressure (SLP) between the eastern and western tropical Pacific (e.g., Bjerknes, 1959; Rasmusson and Carpenter, 1982; Deser and Wallace, 1990; Wang, 2018). Figure 1.1a shows the structure of a positive phase canonical ENSO event. Warm SST anomalies (SSTa) associated with ENSO initiate large areas of deep convection, with the location of the anomalous convection depending on the phase and distribution of SSTa (Tompkins, 2001). As Sardeshmukh and Hoskins (1988), Hoskins and Karoly (1981), Hartmann et al. (1984), Gill (1980), and others have shown, heating within the middle troposphere in the tropics excites Rossby wave trains that propagate into the extratropics, impacting both hemispheres. Consequently, these wave trains modulate atmospheric conditions through a mechanism known as "the Atmospheric Bridge", a well-known pathway through which the tropics can impact conditions in the extratropics (e.g., Wallace and Gutzler, 1981; Deser and Wallace, 1990; Diaz et al., 2001; Alexander et al., 2002).

The atmospheric variability introduced to the extratropics by ENSO links to variability in the Aleutian Low (AL), a semi-permanent area of low-pressure in the North Pacific during boreal winter (Figure 1.2; e.g., Barnston and Livezey, 1987; Yu and Kim, 2011). The atmospheric variability introduced to the extratropics through the atmospheric bridge and the AL also imprint onto the ocean through modulation of SST, sea surface salinity, and mixed layer depth by changing surface heat flux, evaporation, and Ekman transport (Diaz et al., 2001; Alexander et al., 2002; Zhang et al., 2018b; Wills et al., 2019). These anomalies are typically imprinted in the boreal winter season when tropical influence is the strongest, and can persist underneath the
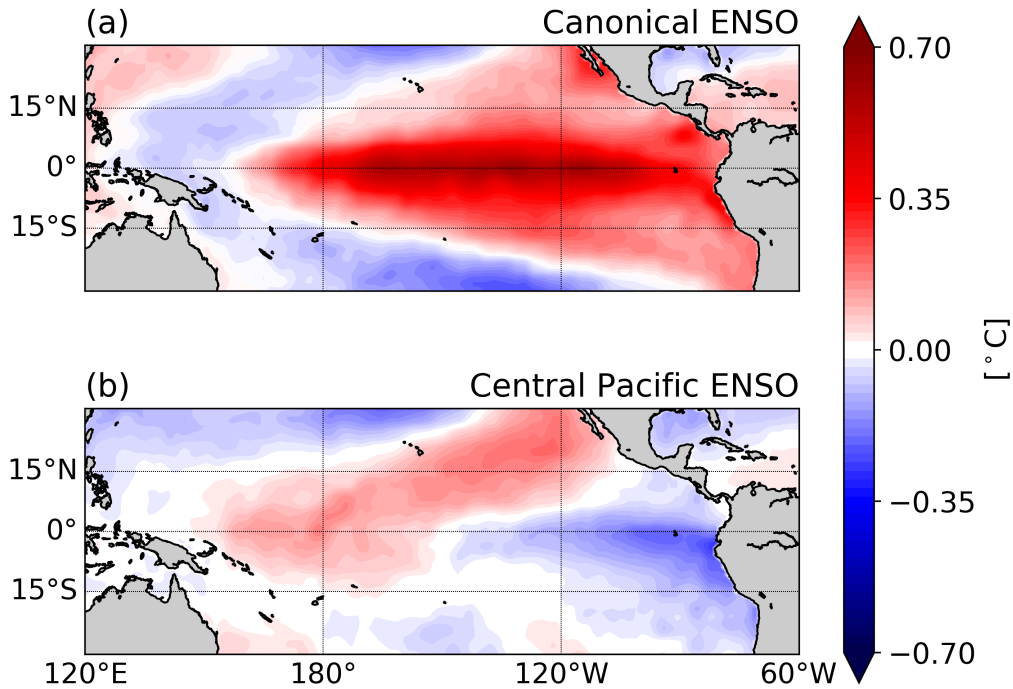
Figure 1.1: The two leading modes of SST variability in the tropical Pacific in HadISST (1870-2019), found by regressing SSTa (°C) onto the first and second principal component time series of monthly mean SSTa averaged over boreal winter (December-February; DJF) after conducting EOF analysis over the domain (30°S - 30°N, 120°E - 60°W). **(a)** is the structure of a canonical ENSO event, the leading mode, and **(b)** is the structure of a CP ENSO event, the second leading mode.

ocean mixed layer until the next winter season through the "reemergence mechanism" (Deser et al., 2003). The imprinting of atmospheric variability onto the ocean during boreal winter and the reemergence mechanism are important in understanding the dynamics and periodicity of the PDO, a mode of climate variability characterized by warm SSTa in the eastern North Pacific and cool SSTa in the western North Pacific during its positive phase (Figure 1.3a; Mantua et al., 1997; Newman et al., 2003; Zhang et al., 2018b). The AL and PDO have been studied extensively for their impacts on storm tracks in the North Pacific (Rodionov et al., 2007; Chu et al., 2020),

marine ecosystems in the North Pacific (Mantua et al., 1997; Bond et al., 2015; Di Lorenzo et al., 2013), and connections to quasi-decadal variability in precipitation over North America (Barlow et al., 2001; Schoennagel et al., 2005; McCabe and Wolock, 2008; Smith et al., 2019). As a result of ENSO, the AL, and the PDO having such large impacts on Pacific climate, accurate seasonal to quasi-decadal predictions of climate variability for the North Pacific and North America are contingent upon understanding and predicting these modes.

The connections between ENSO, the AL, and the PDO allowed scientists to establish a framework for Pacific variability that has improved understanding of seasonal conditions for North America, hereafter referred to as the ENSO-AL-PDO framework (Di Lorenzo et al., 2015). This framework explains a portion of the observed atmospheric and oceanic variability in the North Pacific, however. Other modes of variability are important for a more complete understanding of Pacific variability and seasonal conditions experienced in North America. For example, the primary contributor to extreme winter weather conditions across the midwestern United States during the winter of 2013-2014 was the North Pacific Oscillation (NPO), a climate mode characterized by a north-south oriented dipole in sea level pressure (SLP) anomalies (SLPa) in the North Pacific (Rogers, 1981; Baxter and Nigam, 2015), which is not included in the ENSO-AL-PDO framework. The impacts of this event, in addition to occurrences like the "Warm Blob" (i.e., persistent warm SSTa in the North Pacific; Bond et al., 2015; Hartmann, 2015), motivate researchers to explore Pacific variability outside of the established ENSO-AL-PDO framework.

Secondary modes of variability in the Pacific (ENSO-AL-PDO being the leading modes) have received more attention within the last decade, leading to the establishment of a secondary framework of Pacific variability involving central Pacific (CP) ENSO, the NPO, and the NPGO (i.e., the CP ENSO-NPO-NPGO framework) (Di Lorenzo et al., 2015). CP ENSO events are characterized by a periodic warming and

4
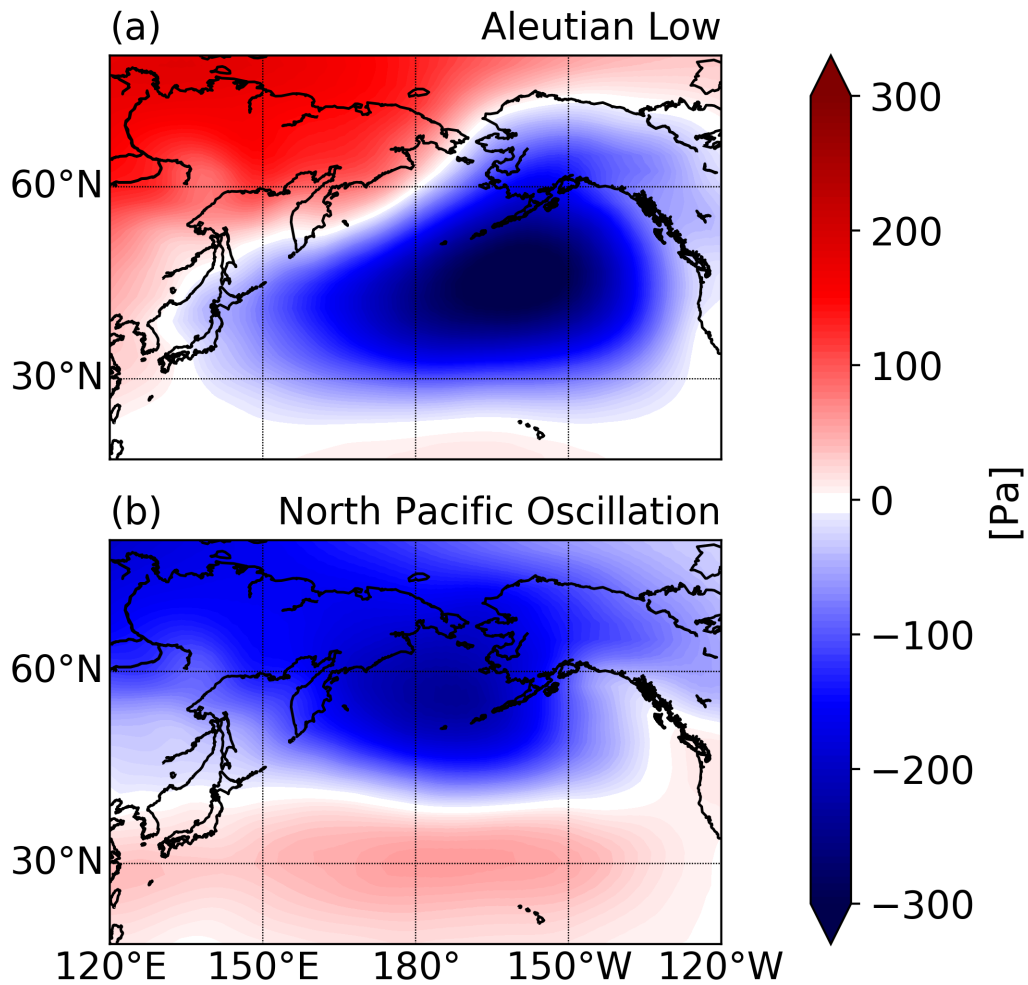
Figure 1.2: The two leading modes of SLP variability in the North Pacific in 20th Century reanalysis (1920-2010), found by regressing SLP anomalies (Pa) onto the first and second principal component time series after conducting EOF analysis on monthly mean DJF SSTa averaged over the domain (15°N - 75°N, 120°E - 120°W). **(a)** is the structure of the Aleutian Low, the leading mode, and **(b)** is the structure of the North Pacific Oscillation, the second leading mode.

cooling of the tropical Pacific, with maximum magnitude SSTa centered near the international dateline (Figure 1.1b; e.g., Ashok et al., 2007), as opposed to the eastern Pacific as with canonical ENSO (Fig. 1.1a). Instead of projecting onto the AL like canonical ENSO, CP ENSO induces variability in the North Pacific on seasonal to
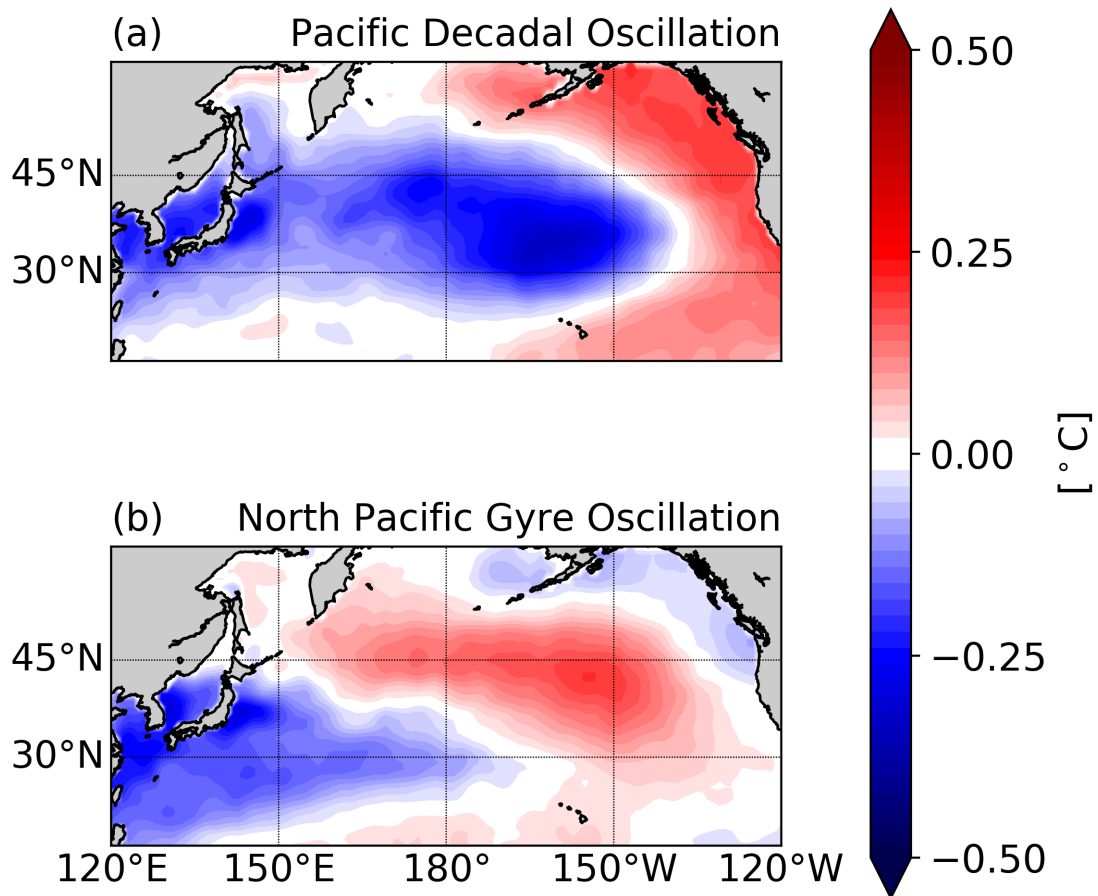
Figure 1.3: The two leading modes of SST variability in the North Pacific in HadISST (1870-2019), found by regressing SSTa (°C) onto the first and second principal component time series after conducting EOF analysis on monthly mean SSTa averaged over DJF for the domain (15°N - 60°N, 120°E - 120°W). **(a)** is the structure of the Pacific Decadal Oscillation (PDO), the leading mode of variability, and **(b)** is the structure of the North Pacific Gyre Oscillation (NPGO) or the "Victoria Mode", the second leading mode.

quasi-decadal timescales via its projection onto the NPO (Figure 1.2b; e.g., Barsugli and Sardeshmukh, 2002; Di Lorenzo et al., 2010; Yu and Kim, 2011; Furtado et al., 2012; Garfinkel et al., 2013; Di Lorenzo et al., 2015; Shi et al., 2019). Further, the

NPO impacts ocean conditions through locally forced surface wind variability (akin to the PDO being the ocean expression of the AL), inducing the NPGO, a northeast-southwest oriented dipole in SSTa also referred to as the "Victoria Mode" (Figure 1.3b; Bond et al., 2003; Di Lorenzo et al., 2008). Studies on the CP ENSO-NPO-NPGO secondary framework for Pacific variability have aided in understanding the dynamics of phenomena such as the "Warm Blob" and persistent drought in California (Bond et al., 2015; Siler et al., 2017). However, further research is required to fully assess the impacts of the modes in this particular framework. Of particular interest are how these secondary modes impact North Pacific and North American climate variability on the quasi-decadal timescale (Liu and Di Lorenzo, 2018; Sun and Okumura, 2019). Motivated by the leading modes of Pacific variability being unable to explain important phenomenon coupled with an interest in decadal-scale hydroclimate variability over the United States, a new mode of quasi-decadal climate variability was recently identified in the North Pacific - the Pacific Decadal Precession (PDP) (Anderson et al., 2016b,a, 2017).

1.2 The Pacific Decadal Precession (PDP)

While most modes of atmospheric climate variability (e.g., AL, NPO) are traditionally thought of as stationary patterns, the PDP is characterized as a cyclonically-propagating lower-tropospheric pressure anomaly dipole around the North Pacific during extended boreal winter, with a full revolution occurring over the course of approximately 12 years (Anderson et al., 2016a). In their investigation of the PDP, Anderson et al. (2016a) separate their discussion of this mode of variability into two phases: a *north-south (N-S) phase* (Fig. 1.4a), when the pressure anomaly dipole is oriented meridionally, and an *east-west (E-W) phase* (Fig. 1.4b) when the dipole is oriented zonally. The evolution of the PDP results in changes in atmospheric circulation over the North Pacific which consequently impact seasonal precipitation and

temperature conditions downstream across North America. With the identification of the PDP, subsequent studies found evidence linking it to decadal variability in precipitation in the Western US (Anderson et al., 2016b,a), marine heatwaves in the North Pacific (Di Lorenzo and Mantua, 2016), and variations in SSTa in the tropical Pacific (Anderson et al., 2016b). These particular phenomena were found to be poorly related to the leading modes of Pacific variability, further motivating research on secondary modes of variability in the Pacific outside of the ENSO-AL-PDO framework.
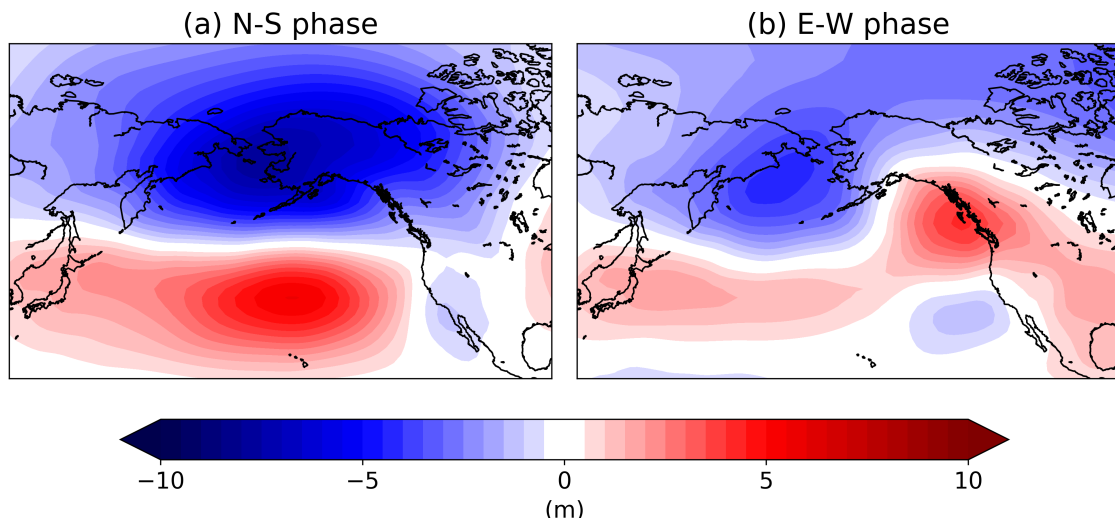
Figure 1.4: Regression of 7-20 year^{-1} band-passed 850 hPa November-March (ND-JFM) averaged monthly mean geopotential height anomalies (m) onto the standardized PDP index at lag -2 years and lag 0 years (negative values mean field leads the PDP index), comprising the **(a)** N-S phase and the **(b)** E-W phase of the PDP for 20th Century reanalysis, respectively.

Establishing an understanding of the dynamics of modes of variability in the North Pacific is particularly important for understanding and predicting their impacts. Indeed, identifying dynamical connections between modes of variability is what led to the leading and secondary paradigms for North Pacific variability (i.e., the ENSO-AL-PDO and CP ENSO-NPO-NPGO frameworks). Currently, the dynamics of the PDP remain unknown. Potential drivers of the PDP are briefly discussed in Anderson et al. (2016a). In addition to separating their analysis of the PDP into two distinct

phases, Anderson et al. (2016a) also differentiate their discussion of the dynamics of the PDP by phase. The hypotheses they propose are:

1) The N-S phase is driven by teleconnections from the central tropical Pacific.

2) The E-W phase is driven by stratospheric temperature deviations through their influence on underlying tropospheric circulations.

Hypothesis (1) relies on the assumption that the N-S phase of the PDP maps onto the NPO (Fig. 1.2). The emergence of the N-S phase of the PDP occurs concurrently with warming and cooling of central tropical Pacific SST, with the pattern of SSTa being reminiscent of CP ENSO (Anderson et al., 2017). Indeed, Furtado et al. (2012) demonstrated that CP ENSO is linked to the NPO, especially the southern node, on quasi-decadal timescales, which would be consistent with this hypothesis should the N-S phase truly map onto the NPO. Taken together, findings from Furtado et al. (2012) and Anderson et al. (2017) support this hypothesis and the possibility for the PDP to fit within the secondary mode paradigm (i.e., the CP ENSO-NPO-NPGO framework; Di Lorenzo et al., 2010, 2015). While previous research supports this hypothesis, a formal analysis investigating a dynamical relationship between CP ENSO and the N-S phase of the PDP has yet to be conducted in reanalysis data or model output.

Hypothesis (2) relies upon previous research showing that tropical Pacific temperature deviations, like those that are associated with the emergence of the N-S phase of the PDP, can induce stratospheric temperature deviations (Iza and Calvo, 2015). Stratospheric temperature deviations can persist after the tropical Pacific temperature deviations subside and induce the E-W phase via downward propagating wave activity (Baldwin and Dunkerton, 1999). In essence, the E-W phase is hypothesized to be a lagged influence from the SSTa pattern in the central Pacific associated with the emergence of the N-S phase of the PDP. Though both hypotheses concerning the

maintenance of the PDP remain untested, this thesis will primarily focus on hypothesis (1) - i.e., the maintenance of the N-S phase.

Research on the PDP and its two phases has primarily used reanalysis data, with only one analysis of atmosphere-ocean coupled global climate model output (Anderson et al., 2017). Of additional and arguably equal importance is characterizing how current state-of-the-art (AOGCMs) capture the PDP and its associated impacts. Indeed, gaining an understanding of how models perform allows for the identification and subsequent improvement of model shortcomings. Historically, AOGCMs have not performed well in simulating Pacific variability, with previous studies showing a wide range in accuracy for both modes of tropical Pacific variability like ENSO (Kim and Yu, 2012; Deser et al., 2017) and modes of North Pacific variability like the NPO (Furtado et al., 2011). The connections between these modes of variability (i.e., through the frameworks introduced in Section 1.1) are weak and even non-existent in some AOGCMs (Furtado et al., 2011; Deser et al., 2012), especially on the quasi-decadal time scale, such that previous studies have drastically increased forcings artificially to produce a robust response (e.g., Shi et al., 2019). Current problems with how AOGCMs simulate Pacific variability present a significant barrier for prediction skill of impacts of natural Pacific climate variability and how Pacific variability may change under a warming climate (Yeh et al., 2009; Di Lorenzo et al., 2010; Furtado et al., 2011; Liu and Di Lorenzo, 2018). However, understanding how current models simulate Pacific variability can provide useful information. Iteratively evaluating AOGCM performance as they are updated helps identify shortcomings and provides the atmosphere-ocean modeling community with improvements on which to focus.

In addition to the importance of investigating dynamical relationships for the PDP to improve understanding and prediction skill for its associated impacts, Anderson et al. (2017) also recognized the importance of identifying how current AOGCMs

capture the PDP. Their initial research into how AOGCMs simulate the PDP using a preindustrial control run of the Community Climate System Model version 4 (CCSM4; Gent et al., 2011) from the Coupled Model Intercomparison Project phase 5 (Taylor et al., 2012) shows that this particular AOGCM did not capture the PDP well. CCSM4 simulates the PDP as a stationary damping and periodic flipping of the N-S phase as opposed to the rotation of a dipole seen in reanalysis data, and does not capture the concomitant evolution of central Pacific SSTa. Results on how one AOGCM simulates the PDP provides limited information on how current models capture it in general. As such, more models need to be analyzed to gain a broad perspective on how current AOGCMs represent the PDP and how they can be improved to increase prediction skill.

1.3   Thesis Goals and Hypotheses

Outlined within Section 1.2 are a series of research gaps which this study aims to fill. Namely, the relationships between N-S phase of the PDP, the NPO, and tropical PDV have not been investigated and very few model simulations of the PDP have been assessed for their performance. The following hypotheses are therefore proposed for this thesis:

1) The N-S phase of the PDP is intimately tied to variability in the NPO.

2) The N-S phase of the PDP is linked to tropical PDV and, specifically, quasi-decadal variations in central tropical Pacific SSTs.

3) AOGCMs show evidence of relationships between the N-S phase of the PDP, the NPO, and tropical PDV.

In parallel to observation-based data, current AOGCMs are also assessed for how they simulate the PDP and the associated SSTa patterns in the central tropical Pacific. Assessing current state-of-the-art AOGCMs is done with the goal of establishing

a broad perspective on how this mode of variability is simulated to identify where current AOGCMs may improve in accurately simulating PDV.

The organization of this thesis is as follows. Data and methods used for this study are included in Chapter 2. Chapter 3 explores the relationship between the north-south phase of the PDP and the NPO in both reanalysis data and AOGCM output. Chapter 4 focuses on relationships between CP SSTa patterns associated with the evolution of the PDP and CP ENSO in all data sets. Finally, a summary and discussion of results is provided in Chapter 5.

Chapter 2

Data and Methods

2.1 Data

Observation-based atmospheric data used in this study are taken from 20th Century Reanalysis version 2 (Compo et al., 2011), Modern-Era Retrospective Analysis and Applications, version 2 (MERRA-2; Gelaro et al., 2017), and the National Center for Environmental Prediction - National Center for Atmospheric Research's Reanalysis-1 (R1; Kalnay et al., 1996). 20th Century data used consists of both monthly-mean geopotential height and SLP on a 2° x 2° latitude by longitude grid, with geopotential height values at 24 pressure levels over the period 1870-2013. MERRA-2 reanalysis data consists of monthly-mean geopotential heights on a 0.5° x 0.625° latitude by longitude grid on 72 hybrid sigma/pressure levels from 1980-2019. R-1 data consists of monthly-mean geopotential heights on a 2.5° x 2.° latitude by longitude grid and 17 pressure levels from 1948-2019. SST data are taken from Hadley Centre's Ice and Sea Surface Temperature data set (HadISST; Rayner et al., 2003), consisting of monthly-mean SST data (1870-2014) on a 1°x1° latitude by longitude grid over the same period. Model output is taken from 500 year (1200 year for CESM2) preindustrial control simulations, in which atmospheric CO_2 concentrations are held to pre-industrial levels so as to eliminate effects of anthropogenic influence, of the Coupled Model Intercomparison Project phase 6 (CMIP6) model runs (Eyring et al., 2016). Model SST data are limited to the first 300 years of each preindustrial control run. SST data are regridded to a 1° x 1° latitude by longitude grid and geopotential height data are regridded to a 2° x 2° latitude by longitude grid, both via bilinear interpolation for all models and reanalysis. More detailed information on the model data used within this study is shown in Table 2.1.

Model Data			
Model	**Institution ID**	**Label**	**References**
ACCESS-CM2	CSIRO-ARCCSS	Australian Community Climate and Earth System Simulator Climate Model Version 2	Dix et al. (2019)
BCC-CSM2-MR	BCC	BCC-CSM 2 MR	Wu et al. (2018)
BCC-ESM1	BCC	BCC-ESM1	Zhang et al. (2018a)
CanESM5	CCCma	Canadian Earth System Model version 5	Swart et al. (2019)
CESM2	NCAR	Community Earth System Model version 2	Danabasoglu et al. (2019)
CESM2-WACCM	NCAR	Community Earth System Model version 2 - Whole Atmosphere Community Climate Model	Danabasoglu (2019)
GISS-E2-1-G	NASA-GISS	GISS-E2.1G	NASA Goddard Institute for Space Studies (NASA/GISS) (2018a)
GISS-E2-1-H	NASA-GISS	GISS-E2.1H	NASA Goddard Institute for Space Studies (NASA/GISS) (2018b)
HadGEM3-GC31-LL	MOHC NERC	HadGEM3-GC3.1-N96ORCA1	Ridley et al. (2018)
MIROC6	MIROC	MIROC6	Tatebe and Watanabe (2018)
UKESM1-0-LL	MOHC NERC NIMS-KMA NIWA	UKESM1.0-N96ORCA1	Tang et al. (2019)

Table 2.2: Information and references for CMIP6 model output used in this study.

2.2 Methods

All data have the long-term monthly-mean removed, and all reanalysis data are linearly detrended to remove potential anthropogenic influence prior to any analysis. Statistical significance of regression and correlation coefficients are determined via a bootstrapping method with 5000 iterations. For each of the 5000 iterations, one time series is randomized prior to conducting either linear regression or correlation. The compilation of these iterations create a distribution against which the true values are tested at the 95% confidence level. Where noted within this study, a 5th order 7-20 year^{-1} Butterworth band-pass filter is applied on a time series to isolate quasi-decadal variability. Any data that is described as "filtered" means it is subjected to an identical 7-20 year^{-1} Butterworth band-pass filter.

The PDP is defined using procedures from Anderson et al. (2017). 850 hPa monthly mean November-March (NDJFM) averaged geopotential height anomalies over the North Pacific $(15 - 80°\text{N}, 125°\text{E-90}°\text{W})$ are band-pass filtered from 7-20 years^{-1} and then subjected to singular value decomposition (SVD). The analyzed monthly mean geopotential height anomalies are isolated to NDJFM as the PDP is primarily active during the extended boreal winter season Anderson et al. (2017). The leading mode resulting from the SVD (i.e., the pattern associated with the AL) is then linearly removed from the height field via linear regression. The residual spatio-temporal matrix is extended by 5 one-year lags prior to employ time-extended SVD. Decomposing the time-lagged spatio-temporal matrix using this method allows for the identification of potentially-propagating modes of variability. Regressing the filtered anomaly field onto the leading principal component time series from the time-extended SVD at the appropriate lags yields a sequence of 6 maps representing the progression of the PDP over a 6 year period. Following Anderson et al. (2017), the third map in this series is designated as Year 0, with the first two maps "leading" and last three maps "lagging" this central map. The leading principal component time

series is hereafter referred to as the PDP index, and is the *average* of the time series of the 6 maps describing the evolution of the PDP.

An EOF-based approach outlined by Kim and Yu (2012) is used to define canonical ENSO and CP ENSO structure. Influence from SSTa in the Niño4 region (5°S - 5°N, 160°E-150°W) is removed from -3 to +3 months using multilinear regression to isolate SSTa associated with canonical ENSO. The same multilinear regression method is applied to isolate SSTa associated CP ENSO, except the influence from the Niño1+2 region (10°S - 0°, 90°W-100°W) is removed instead of the Niño4 region. After subjecting the residuals for each to SVD analysis, the leading EOF is then multiplied by the square root of the associated eigenvalue to arrive at the standard deviations in the leading EOF of tropical Pacific SSTa associated with canonical ENSO and CP ENSO. The resulting patterns are therefore indicative of the SSTa structure for canonical ENSO and CP ENSO events. The domain over which the SVD analysis is conducted for each analysis is (30°S - 30°N, 120°E-60°W).

Power spectrum analyses are conducted on the entirety of available data for HadISST and the first 300 years of output for each model included in this study. Each dataset is separated into 3 overlapping subsets. More specifically, the dataset is split in half and the third subset is an overlapping segment centered on the middle of the data set. This method of dividing the data was chosen in order to apply a Hanning window to the time series, which resulting in a partial loss of data at the end of the time domains for each subset. After the Hanning windows are applied the subsets each decomposed into their power spectrum. The three power spectra are subsequently averaged together. This Hanning window method was chosen to increase the degrees of freedom the power spectrum prior to testing for statistical significance. All power spectra are tested at the 95% confidence level using chi-squared

testing using *a priori* statistics. Use of *a priori* statistics is warranted as both canonical and CP ENSO have been shown to have power on interannual to decadal time scales (Diaz et al., 2001; Furtado et al., 2012; Wang, 2018).

Chapter 3

The PDP and NPO in Reanalysis and Model Output

3.1 Identifying the PDP in reanalysis data

The full evolution of the PDP using 20th Century reanalysis data can be seen in Figure 3.1. Figs. 3.1a,b,e,f represent the N-S orientation of the pressure dipole associated with the PDP, while Figs. 3.1c,d are represent the E-W phase. Signs of precession can be seen throughout the series of maps, with the positive anomaly comprising the northern pole of the PDP at Year -2 rotating counter-clockwise to become the western pole at Year 0 and the southern pole at Year 2. These results follow those shown within Anderson et al. (2017) for 20th Century Reanalysis as well.

To justify continual use of 20th Century Reanalysis data throughout this study, the evolution of the PDP index from 20th Century Reanalysis is checked against the PDP index from Reanalysis-1 (R-1) and MERRA-2 data. Figure 3.2 shows the PDP index for each of these data sets. Similar to the time series shown within Anderson et al. (2017), the 20th Century PDP index show a period of quiescent activity until the mid 1980s, when the variance increases notably. Both R-1 and MERRA1 indexes show similar heteroscedasticity, tracking 20th Century data well throughout their respective time domains. Indeed, when the PDP indexes are correlated with each other for the time domains on which they overlap, all correlation coefficient values exceed 0.9 and are statistically significant ($p \ll 0.001$). In response to the high degree of similarity in these time series, the analyses throughout the remainder of this chapter focuses solely only 20th Century reanalysis data. This particular data set is chosen as it has the longest record of the three shown in Fig. 3.2 and is used in previous literature to investigate the PDP which facilitates easier comparison to previous work (Anderson et al., 2016a, 2017).
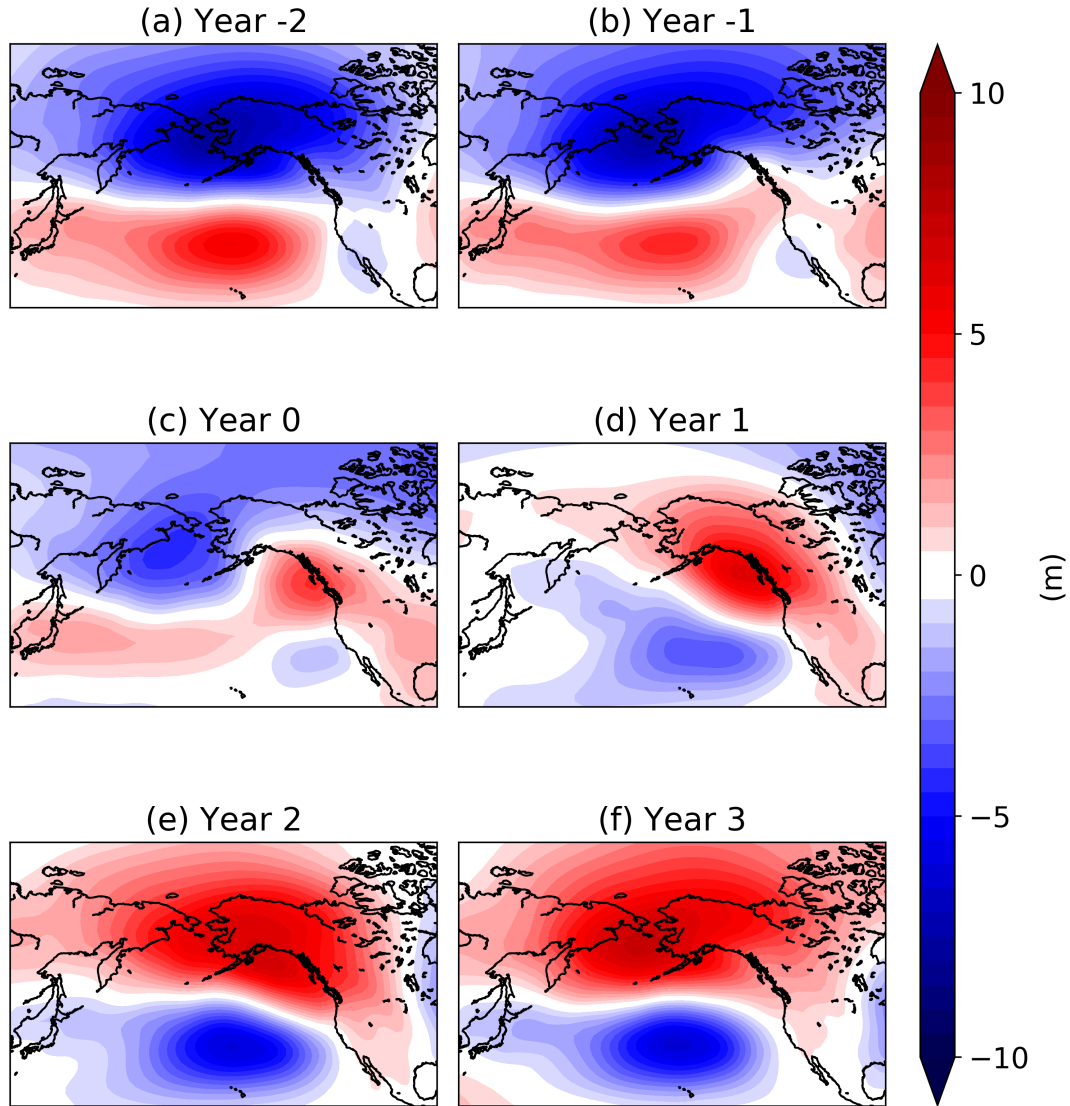
Figure 3.1: Regression of 7-20 year^{-1} band-pass filtered 850 hPa NDJFM averaged monthly mean geopotential height anomalies (m) onto the standardized PDP index at 6 different lags for 20th Century reanalysis. The third map is defined as Year 0 following methods from Anderson et al. (2017)

3.2   Relating the PDP and the NPO

The first hypothesis proposed for this study - i.e., the N-S phase of the PDP maps onto the NPO, is investigated by first defining an index to track the NPO, following methods from Furtado et al. (2012), and filtering it to isolate quasi-decadal variability.
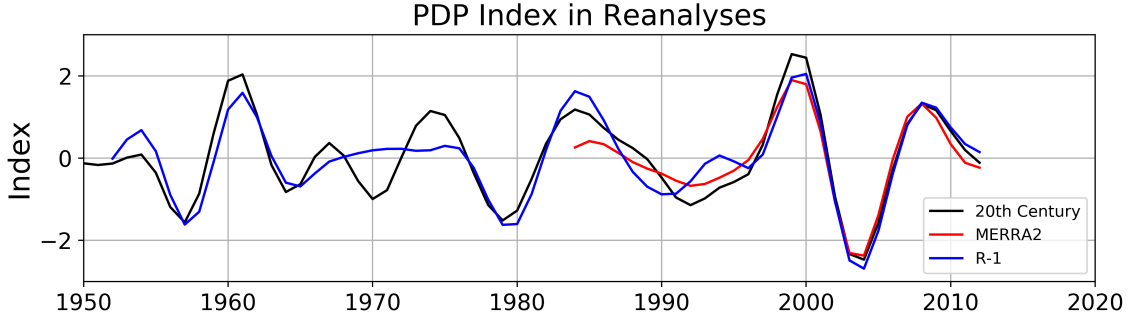
Figure 3.2: Comparison of the standardized PDP index from 20th Century Reanalysis (20th Century; black line), MERRA-2 (red line), and NCEP-NCAR R-1 (blue line)

The index is created by area-averaging NDJFM-averaged monthly mean SLPa that encompasses the south pole (SP) of the NPO (15° - 27.5°N, 175°E - 147.5°W) and subtracting this from an area-averaged SLPa over the north pole (NP) of the NPO (55° - 72.5°N, 180° - 140°W); i.e.,

$$NPO_{Index}(t) = NPO_{NP}(t) - NPO_{SP}(t) \tag{3.1}$$

Figure 3.3 shows the correlation of SLPa with the filtered NPO index for 20th Century reanalysis overlaid with the domains used for the NP and SP. The highest correlation values reside within the NP and SP domains used to find the NPO Index, which justifies the use of this particular index to track the NPO.

A direct comparison of the PDP index and the NPO index is shown in Figure 3.4. The NPO index tracks the PDP index well throughout their shared time domain, with a correlation coefficient of $r = 0.67$ ($p \ll 0.01$). The NPO index correlates well with the PDP index when both have large magnitudes, but the two tend to diverge when the PDP index is small in magnitudes (i.e. ~1920 - mid 1980s). The reason for this is unclear, though it could be a statistical artifact arising from the PDP index being the average of the six time series tracking the evolution of the PDP from Fig. 3.6. While the NPO index and the PDP index show signs of a relationship, the NPO index only explains ~45% of the variance in the PDP index. Taken together, the
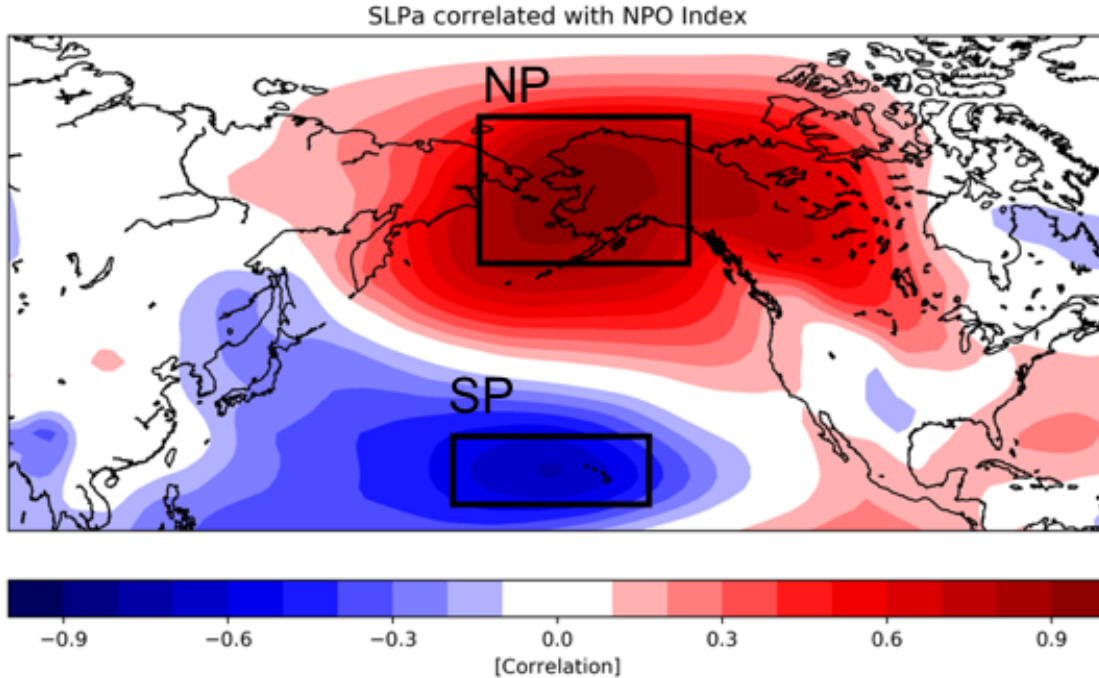
Figure 3.3: Correlation of SLPa (Pa) in the Pacific with the NDJFM averaged 7-20 year^{-1} band-pass filtered NPO Index for 20th Century Reanalysis from 1880-2013. Overlaid are the domains for the NP (55° - 72.5°N, 180° - 140°W) and SP (15° - 27.5°N, 175°E - 147.5°W) used to create the NPO Index.

moderate variance explained by the NPO index and periods where the two indices do not track each other imply that the PDP cannot solely be explained by the NPO index. This also indicates that the PDP is a robust mode of variability and not merely the quasi-decadal expression of the NPO.

To further investigate how low-frequency variability in the NPO is related to the N-S phase of the PDP, NDJFM averaged monthly mean filtered 850 hPa geopotential height anomalies onto the filtered NPO index at lags 0 to 5 years (field lagging the NPO index; Figure 3.5) to investigate whether the NPO index explains enough variability in the PDP to capture its full evolution. The precession of the PDP over the 6 maps shown in Fig. 3.5 is largely recovered, though there is a notable difference from the evolution of the PDP in Fig. 3.6. The N-S phase is clearly represented in Figs. 3.5a,b,e,f and the E-W phase is distinct in Fig. 3.5c, however the western pole
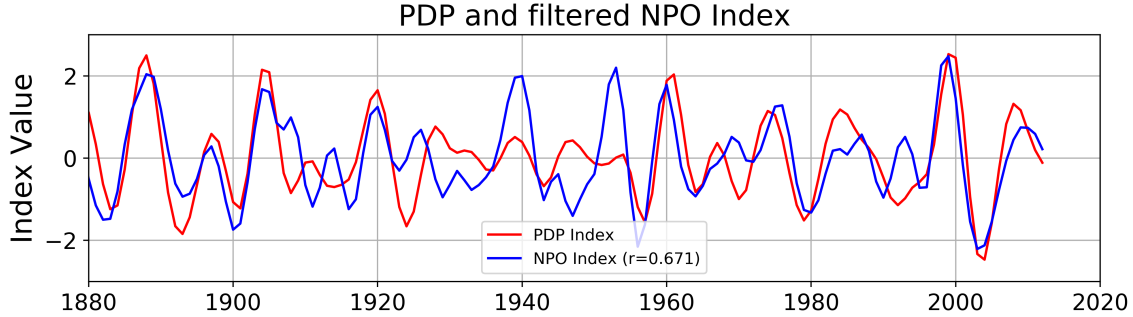
Figure 3.4: Time series of comparing the PDP Index and the NPO Index NDJFM averaged 7-20 year^{-1} band-pass filtered NPO Index for 20th Century Reanalysis from 1875-2013. Value in parenthesis is the correlation coefficient between the PDP Index and the filtered NPO Index.

of the E-W phase in Fig. 3.5d is not captured. Thus, the large fraction of variance in the PDP's evolution that is not explained by the NPO index is likely a result of the NPO index not capturing variability associated with the E-W phase of the PDP. Regardless, the high correlation between the NPO index and the PDP index along with the recovery of the majority of the PDP's precession from the lag regressions strongly support that the N-S phase of the PDP is related to NPO.

3.3 The PDP in CMIP6 Models

After establishing that the N-S phase of the PDP is related to the NPO on the quasi-decadal timescale in reanalysis data, this next section focuses on model output from the CMIP6 suite to identify how current AOGCMs simulate the PDP with specific focus on how they simulate the N-S phase. As discussed briefly within Chapter 1, understanding how current AOGCMs simulate Pacific variability can inform of biases within current models. Subsequent improvement of these biases improves climate prediction on a wide range of timescales, and is therefore important to identify them.

Figure 3.6 displays the structure of the PDP in preindustrial control simulations of the CMIP6 models used in this study, which are found using the same time-extended SVD analysis used for reanalysis. In general, output from the CMIP6 models used

22
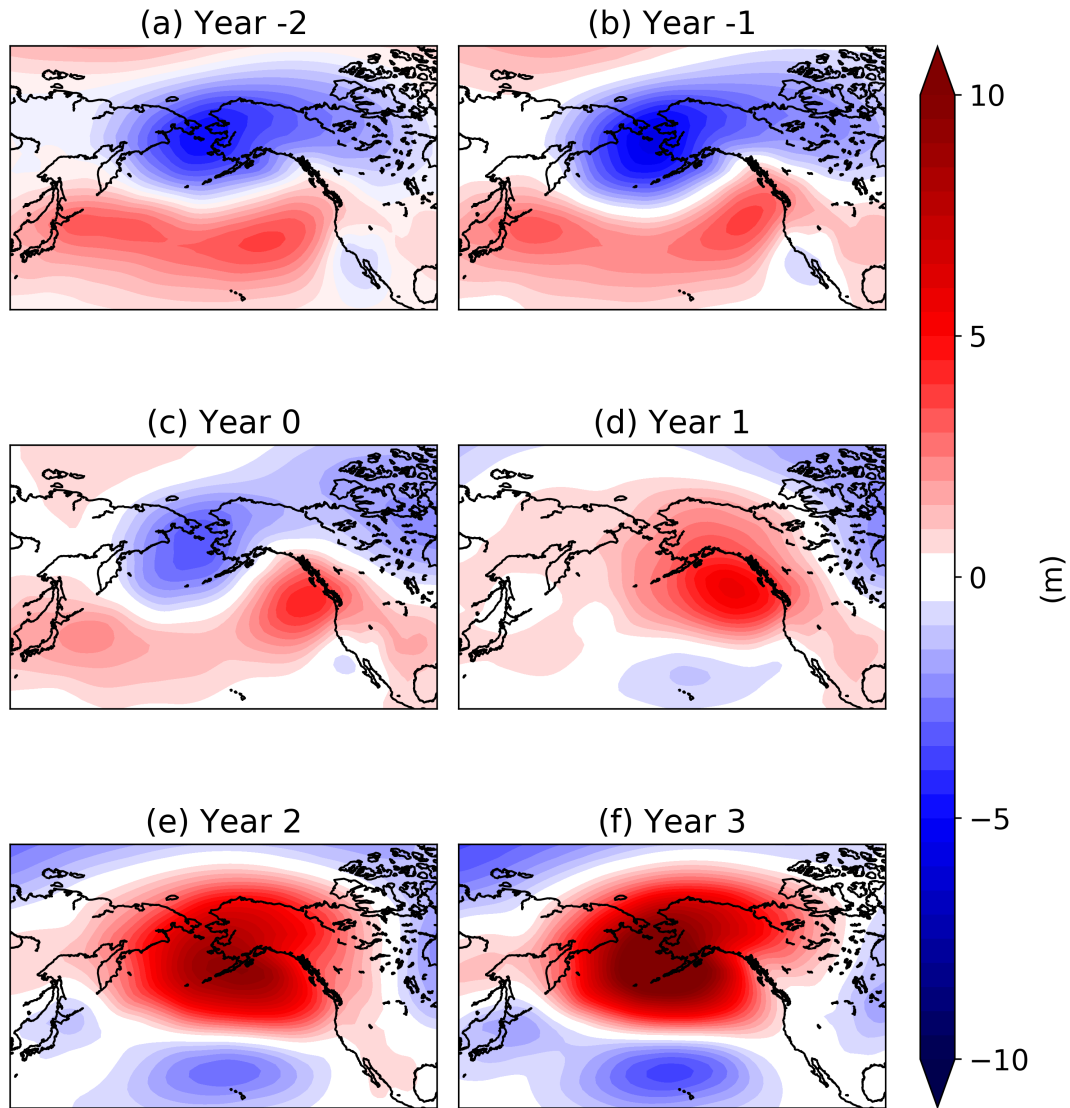
Figure 3.5: Regression of NDJFM averaged 7-20 year^{-1} band-passed 850hPa monthly mean geopotential height anomalies onto the filtered NPO Index from 0 to 5 lags. The third map in this series is defined to be Year 0 to facilitate easier comparison with the PDP.

in this study capture the N-S phase of the PDP adequately (Fig. 3.6a,b,e,f; Years -2, -1, 2, 3), though the location, extent, and magnitude of the anomaly dipole varies across models. For example, the northern pole of the PDP within GISS-E2-1-G is larger in magnitude than in 20th Century Reanalysis and is situated farther west in the North Pacific (Fig. 3.6, Year 2). CESM2 simulates the northern pole with a
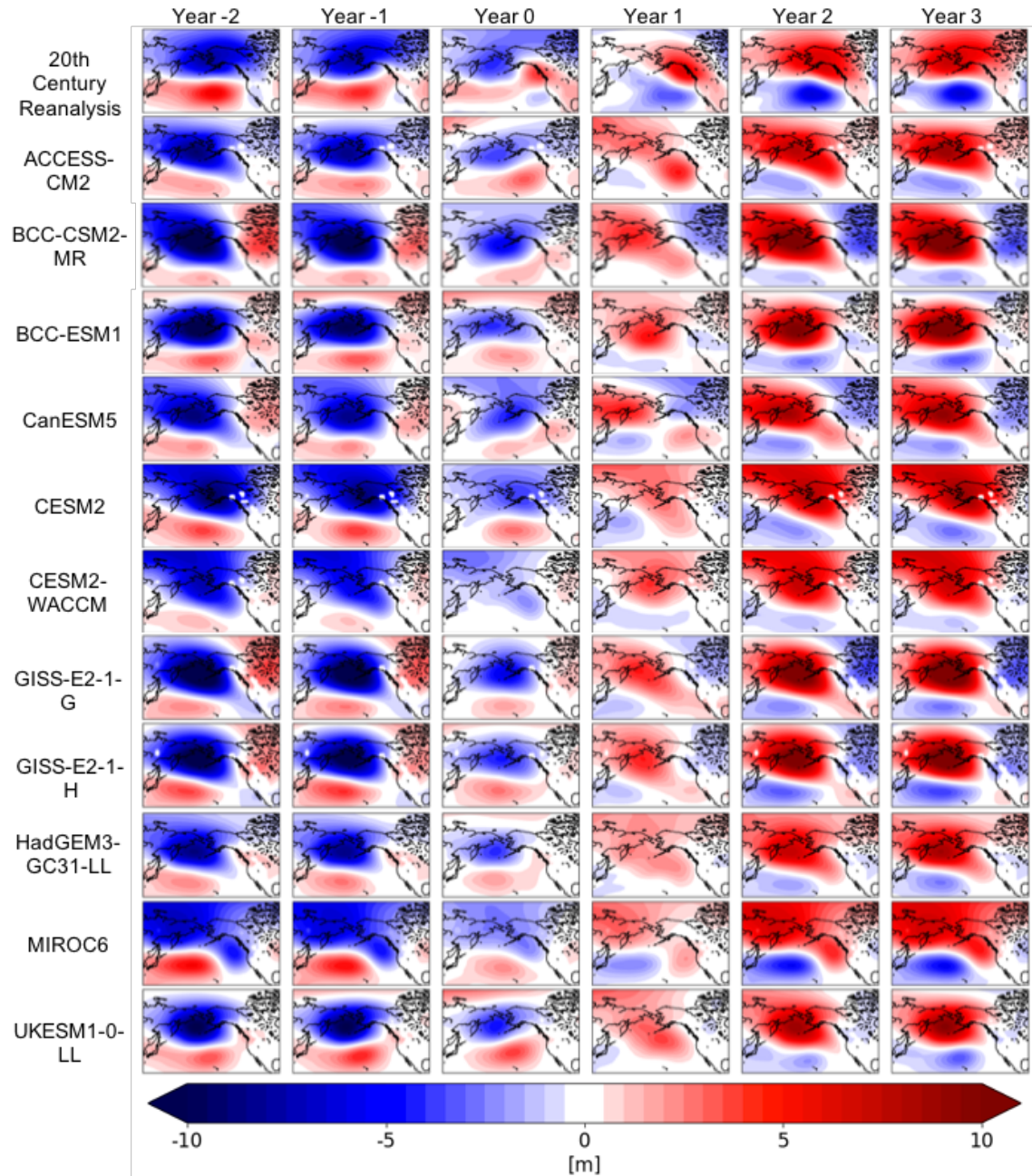
Figure 3.6: Regression of 7-20 year^{-1} band-passed 850hPa NDJFM averaged monthly mean geopotential height anomalies (m) onto the standardized PDP index at lags 0 to 5 (PDP index leading geopotential height anomalies) for 20th Century Reanalysis and all model output. The third map in each progression as Year 0, following methods from Anderson et al. (2017)

northwesterly extension of the anomaly not seen in 20th Century Reanalysis, nor is

the southeasterly extension shown in MIROC6. More importantly, while reanalysis

includes a distinct E-W phase of the PDP, models struggle to accurately capture this intermediary phase, with only a few showing evidence of a distinct E-W phase (Fig. 3.6c,d; Years 0,1). ACCESS-CM2 and CESM2-WACCM include evidence for some precession, shown by slight cyclonic rotation of the anomaly dipole, though the magnitude of the anomaly dipole for the E-W phase is much less than in reanalysis. Several others, including UKESM1-0-LL and BCC-ESM1, show more evidence for the north-south phase damping and reversing sign as opposed to precessing cyclonically.

The results from Anderson et al. (2017) for the PDP in CCSM4 are representative of the AOGCMs analyzed within this study; i.e., most models poorly represent the E-W phase. Given that Anderson et al. (2016a) connected the E-W phase of the PDP to quasi-decadal drought/pluvial cycles across the western US, simulations of the E-W phase of the PDP is an area of much needed improvement in current AOGCMs to increase prediction skill for drought/pluvial conditions. Previous results in Section 3.2 suggesting that variability in the E-W phase of the PDP is not captured well by the NPO places this problem outside of the scope of this thesis. The importance of studying the E-W phase will be revisited in Chapter 5.

In order to summarize the model results more succinctly, the performance of all models' representation of the N-S phase during Year 2 is compared quantitatively. Year 2 was chosen as it includes a distinct N-S phase in all models (Fig. 3.6, Year 2) and coincides with significant warm anomalies in central tropical Pacific surface and subsurface temperatures in reanalysis (Anderson et al., 2016a, 2017). We next create an index of the N-S phase of the PDP which allows for the comparison of anomaly magnitude between model and reanalysis results. Referred to as the N-S index, it is defined as the area-averaged 7-20 year^{-1} band-pass filtered 850 hPa monthly mean geopotential height anomalies encompassing the southern node of the dipole (20°N - 40°N, 175°W - 145°W) subtracted from that of the northern node (50°N - 70°N, 175°W - 130°W). This index is quite similar to the NPO index defined in Section
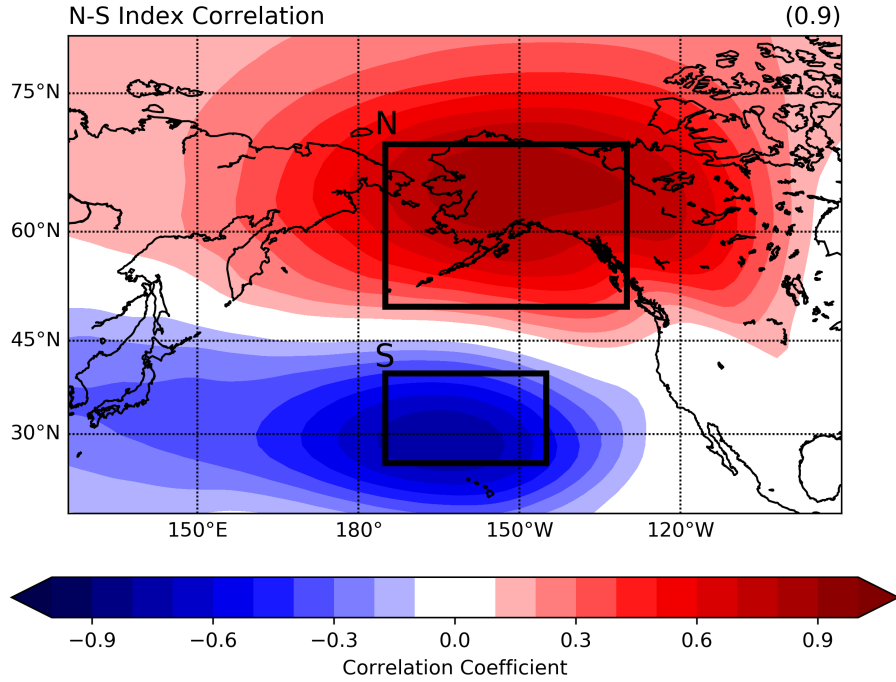
Figure 3.7: Correlation of 7-20yr^{-1} band-passed 850hPa NDJFM averaged geopotential height anomalies with the N-S Index. Black boxes designate the northern (N) (50°N - 70°N, 175°W - 130°W) and southern (S) (20°N - 40°N, 175°W - 145°W) domains used to define the N-S Index. Value in parenthesis in upper right is the spatial correlation with the PDP Year 2 map.

3.2, except with slight differences in the areal domain. Fig. 3.7 shows the correlation of the 7-20 year^{-1} band-pass filtered 850hPa geopotential height anomalies over the domain with the N-S index. Maximum correlation values residing within the domains used to create the N-S index, as well as the spatial correlation with the Year 2 map ($r = 0.9$), indicates the N-S index captures both nodes of the north-south phase of the PDP well (Fig. 3.6, top row, Year 2).

In addition to measuring variability in the anomalies at Year 2, spatial correlations for each model Year 2 map from Fig. 3.6 are computed with reanalysis to determine how similar each is to the N-S phase of the PDP in observation. These metrics are captured in a Taylor diagram (Figure 3.8). The Taylor diagram shows that most
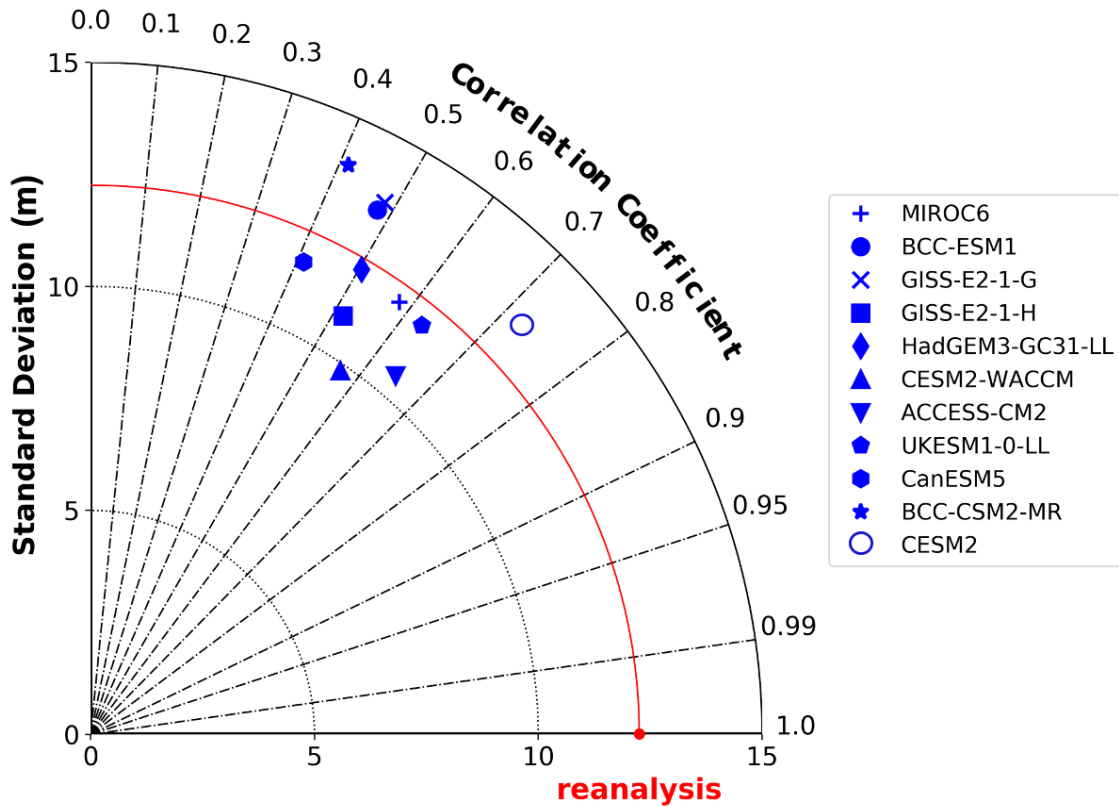
Figure 3.8: Taylor diagram of model output relative to 20th Century Reanalysis. The standard deviation measure (m) is derived from the N-S index and the correlation coefficient is computed spatially for the Year 2 maps from Fig. 3.6 relative to 20th Century reanalysis.

models under-simulate the observed variability in the N-S phase, especially CESM2-WACCM, suggesting that the N-S phase of the PDP within modes has magnitude less than observed. Spatially, excluding CESM2, no model has a correlation with the 20th Century Reanalysis map greater than $r = 0.7$, with most residing between $r = 0.4$ and $r = 0.6$. The low correlation values highlight that model simulations of the north-south phase, while successfully capturing the PDP's dipole in atmospheric pressure, struggle with replicating the same orientation and extent of the anomalies at lag 2 years. To summarize the results from Fig. 3.8, CESM2, ACCESS-CM2, and UKESM1-0-LL perform the best based on their spatial correlation, with CanESM5 and BCC-CSM2-MR performing the worst. For the magnitude of the N-S phase

(i.e., the standard deviation in the N-S index), HadGEM3-GC31-LL and MIROC 6 perform the best with CESM2-WACCM and BCC-CSM2-MR performing the worst.

3.4   Chapter Summary & Discussion

The results within Section 3.2 show that the PDP is related to the NPO on quasi-decadal timescales. This finding is supported by the highly significant correlation between the NPO index ($r = 0.67$; Fig. 3.4) and the lag regressions involving the NPO index recreating much of the PDP's evolution (Fig. 3.5). The implications of these findings are that the secondary mode paradigm (i.e., CP ENSO-NPO-NPGO) indirectly includes variability associated with the PDP with the inclusion of the NPO, as the PDP is related to the quasi-decadal expression of the NPO. Yet, these findings also highlight that the secondary mode paradigm may be incomplete on the quasi-decadal time scale. The NPO index does not entirely explain the variability in the PDP, likely due to the NPO index not capturing the variability in the E-W phase of the PDP during its transition to the N-S phase, as seen in Fig. 3.5d. The inability of NPO index in explaining variability associated with the E-W phase of the PDP means that the E-W phase is likely to have a different dynamical driver than the N-S phase of the PDP, and therefore will require a separate investigation into what forces it.

After connecting the N-S phase of the PDP to the NPO in Section 3.2, Section 3.3 assessed model performance in simulating the PDP with specific focus on the N-S phase. Overall, the results for CMIP6 model output suggest that coupled climate models struggle with accurately capturing the PDP both in spatial signature and magnitude, especially the E-W phase. A potential reason for this, which will be assessed further in the next chapter, could be that models do not accurately capture the interactions between the secondary climate mode paradigm for the North Pacific (i.e., the CP ENSO-NPO-NPGO framework). Furtado et al. (2011) assessed how

models in the Intergovernmental Panel on Climate Change (IPCC) Fourth Assessment Report (AR4) captured decadal variability in the North Pacific and found that most models failed to replicate the observed connection between CP ENSO and quasi-decadal NPO variability. Should the N-S phase of the PDP be influenced by CP ENSO, then the inability of models in capturing the connection between the central Pacific and the North Pacific would assuredly introduce errors into their simulations of the PDP.

As a result of the PDP not being solely quasi-decadal fluctuations in the NPO, the secondary mode framework (i.e., CP ENSO-NPO-NPGO) for Pacific variability may be incomplete. The relationship between the PDP and quasi-decadal variability in the NPO uncovered here supports the need to add the PDP to this paradigm. In what way the PDP will need to be added remains to be seen. More understanding of the dynamics of the N-S phase and E-W phase need to be established prior to confidently placing the PDP within this paradigm. A relationship that was briefly discussed within Chapter 1, and one which motivates the second hypothesis of this thesis, was that the NPO is linked to fluctuations in CP ENSO (Di Lorenzo et al., 2010; Furtado et al., 2012). Indeed, both CP ENSO and the NPO (especially the southern pole) have significant power on quasi-decadal timescales (Furtado et al., 2012). This periodicity matches the dominant quasi-decadal period of the PDP. Further, both Anderson et al. (2016a) and Anderson et al. (2017) tied the emergence of the N-S phase of the PDP to fluctuations in surface temperature and subsurface temperature anomalies in the central tropical Pacific. Given the demonstrated linkage between the PDP and the NPO on quasi-decadal timescales and the shared timescales between the NPO, the PDP, and CP ENSO, there is a considerable possibility that the PDP is both related to and partially driven by central tropical Pacific SST variability. The next chapter will build on these previous results and search for evidence of a linkage between the N-S phase of the PDP and CP SSTa. Results from CMIP6 model output

will be assessed simultaneously to give context on how current models capture any relationship between the N-S phase of the PDP and CP ENSO with the goal of identifying necessary model improvements to simulate the PDP.

Chapter 4

The PDP and Tropical Pacific Climate Variability

The following chapter examines how the PDP is related to central Pacific SSTs to investigate how the PDP may fit within the secondary mode paradigm for Pacific variability. Preliminary results from Anderson et al. (2016a) and Anderson et al. (2017) show the central tropical Pacific undergoing warming and cooling during the emergence of N-S phase of the PDP. They hypothesized that the warming and cooling patterns in the central Pacific may dynamically drive the N-S phase of the PDP. Here this hypothesis will be investigated further using both reanalysis and model output by comparing the concomitant SSTa evolution in the central Pacific during the emergence of the N-S phase of the PDP and the two leading modes of boreal wintertime variability in SSTa in the tropics: canonical ENSO and CP ENSO.

4.1   Signals in the Pacific

Figure 4.1 shows the regression of NDJFM averaged SSTa in the tropical Pacific from HadISST data onto the PDP index from 20th Century Reanalysis at various lags. Fig. 4.1 demonstrates the evolution of SSTa in the tropical Pacific associated with variations in the PDP index. Much like results from Anderson et al. (2016a), warming of the central tropical Pacific occurs with the transition of the PDP from the E-W phase to its N-S orientation (Fig. 4.1def). More specifically, the Year 1 pattern (SSTa lagging the PDP index, Fig. 4.1e) results in a similar broad area of significant positive SSTa throughout the central tropical Pacific shown by Anderson et al. (2017), with an additional area of negative SSTa confined to the western Pacific. Interestingly, this SSTa pattern suggests that most of the eastern tropical Pacific experiences warming in addition to the central Pacific, which is more indicative of canonical ENSO conditions.

While Anderson et al. (2017) hypothesized that the SSTa pattern associated with the emergence of the N-S phase of the PDP is related to CP ENSO, the pattern shown in Fig. 4.1e may provide evidence that the SSTa pattern could in fact be a decadal expression of canonical ENSO. As the warm signal is the strongest within the Year 1 SSTa pattern, the focus of the rest of this chapter will be on this particular pattern in both reanalysis and model output.
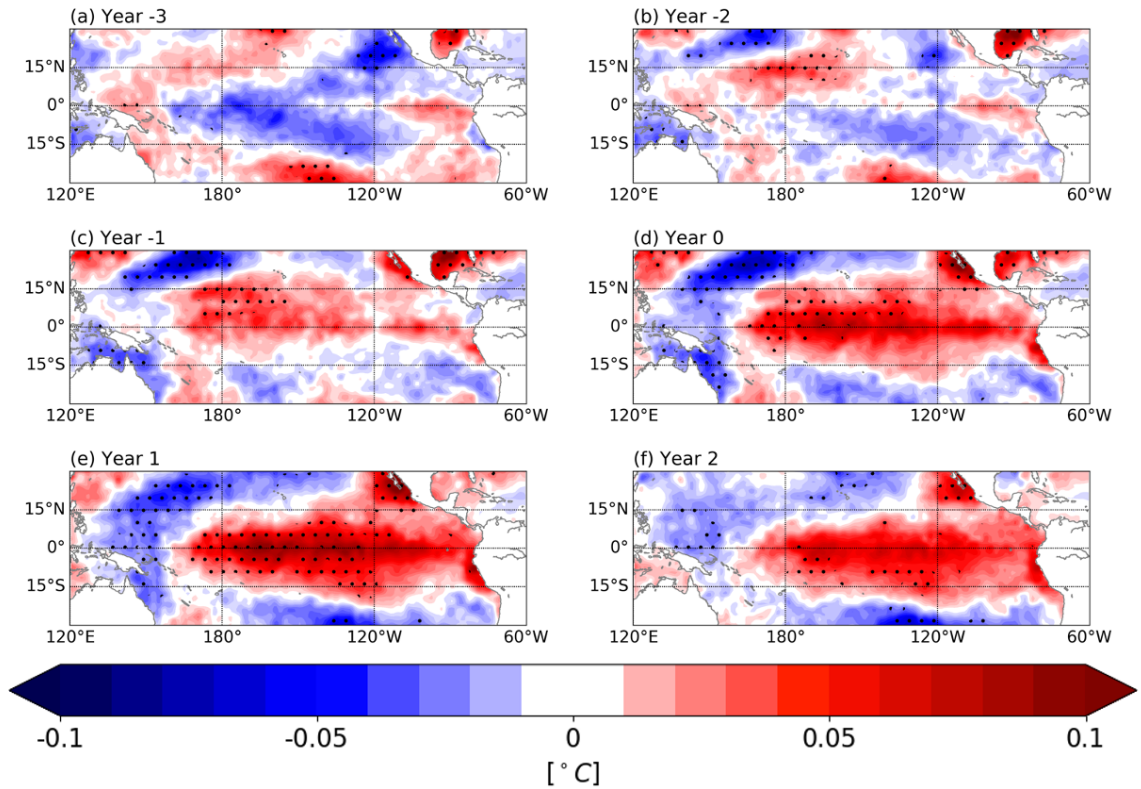
Figure 4.1: Regression of NDJFM averaged SSTa ($°C$) in the tropical Pacific onto the PDP Index from lags **(a)** -3 years to **(f)** 2 years using SST data from HadISST and the PDP index from 20th Century Reanalysis. Positive (negative) year indicate the PDP index leads (lags) SSTa. Stippling denotes statistically significant regression coefficients at the 95% confidence level using a bootstrapping method with 5000 iterations.

Transitioning to model output, Figure 4.2 shows the regression of SSTa onto the PDP index at lag Year 1 (SSTa field lagging the PDP index) for several CMIP6 models in order to investigate how models capture the SSTa pattern in reanalysis. The Year 1 SSTa patterns show little consistency between model and reanalysis results, with

only BCC-ESM1 showing evidence for a significant relationship between warm central Pacific SSTa and the N-S phase of the PDP. That said, the pattern in BCC-ESM1 is much more indicative of canonical ENSO, with warm anomalies extending into the eastern tropical Pacific as well. CESM2 and CESM2-WACCM (Fig. 4.2bh) show warm anomalies in the central Pacific, however these anomalies are largely insignificant at the 95% confidence level. Both MIROC6 and BCC-CSM2-MR show statistically significant *negative* SSTa associated with this phase of the PDP, while the rest of the models used in this study show no consistent statistically significant SSTa structure. If CP ENSO is indeed dynamically linked to the PDP at this phase, then the lack of consistency in how the models capture the SSTa pattern in the central Pacific at Year 1 suggests that models do not replicate this relationship. Further, if the N-S phase of the PDP is linked to SSTa in the tropical Pacific, then model performance in replicating the associated SSTa may be a potential explanation for why models diverge from reanalysis on their representations of the N-S phase.

The SSTa pattern observed during the north-south phase of the PDP at lag +1 year (i.e., Year 1) is reminiscent ENSO events, with the maximum anomaly located in the central Pacific and cold anomalies in the western Pacific (Ashok et al., 2007). Anomalies also extend toward the southwestern coast of North America, which is characteristic to both CP ENSO events and extratropical influence that can be associated with canonical ENSO events (Vimont et al., 2003). The similarities between the CP ENSO spatial pattern from Ashok et al. (2007) (see also; Fig. 1.1) and the regression results from HadISST in Fig. 4.2 lead us to investigate whether low-frequency variance in either canonical ENSO or CP ENSO events are associated with the transition to the north-south phase of the PDP at Year 1. Should this pattern truly be associated with CP ENSO, past literature detailing how models struggle with capturing Pacific SST variability (see; Kim and Yu, 2012) could explain why models are not capturing the SSTa pattern at Year 1.

4.2 Relationship to Tropical Pacific Variability

To examine how the SSTa pattern at Year 1 is related to canonical ENSO and CP ENSO, an EOF-based approach is used to identify canonical ENSO and CP ENSO structure. The method used here utilizes multi-linear regression to remove the influence of SSTa from the central Pacific for canonical ENSO and from the eastern Pacific for CP ENSO prior to conducting EOF analysis (see Kim and Yu, 2012). The EOF-based approach yields a structure that is similar to previous results investigating both canonical ENSO (Figure 4.3a) and CP ENSO (Figure 4.4a) in HadISST data (Ashok et al., 2007; Kim and Yu, 2012). For canonical ENSO, the location of maximum variability is confined to the eastern Pacific, while the location of the maximum anomalies for CP ENSO is located more in the central Pacific. The CP ENSO structure in Fig. 4.4a shows an extension of larger magnitude variability extending toward the coast of southwestern North America, which is more similar to the structure of the SSTa pattern at Year 1 (Fig. 4.1e) than the SSTa variability structure shown in Fig. 4.3 for canonical ENSO.

Comparing model simulations of canonical ENSO to results from reanalysis shows some considerable differences. Some models, such as GISS-E2-1-G (Fig. 4.3i) and MIROC6 (Fig. 4.3l) have much more variability in SSTa associated with canonical ENSO events. Additionally, the spatial structure varies from model to model as well, with spatial correlations between model and reanalysis ranging from $r = 0.69$ (CanESM5; Fig. 4.3d) to $r = 0.89$ (CESM2; Fig. 4.3b). Because ENSO is linked to the AL and PDO, the variability in canonical ENSO representation here suggests that models likely misrepresent the influence of SSTa in the tropics on modes of climate variability in the North Pacific as well. Further, since both the AL and PDO influence North Pacific and North American climate, models are also likely to misrepresent their impacts.

The model results for CP ENSO structure show the location of maximum SSTa variability in most models is eastward of the location shown in reanalysis data, which is more reminiscent of canonical ENSO events where the maximum SSTa variability is typically confined to the eastern Pacific. CESM2 and CESM2-WACCM (Fig. 4.4b,h) are an exception to this, with maximum positive SSTa farther west than in HadISST. The results for CP ENSO further highlight how models struggle with accurately capturing SSTa variability in the tropical Pacific. These errors will likely impact to the teleconnection patterns associated with both canonical ENSO and CP ENSO. If the N-S phase of the PDP is dynamically linked to canonical ENSO or CP ENSO, then models struggling to accurately simulate ENSO or CP ENSO will certainly impact how models represent the evolution and structure of the N-S phase of the PDP.

The PDP is a quasi-decadal mode of variability and, as such, a relationship with SSTa in the tropical Pacific should vary on a similar time scale (i.e., ∼7-20 years). Therefore, analyses of the power spectra of the time series for both canonical and CP ENSO are conducted to identify their dominant periods. Figure 4.5 shows the results from power spectrum analyses on the principal component time series describing canonical ENSO resulting from the SVD analysis from Fig. 4.3 for both reanalyses and CMIP6 model output. As expected, reanalysis data and all model output have significant peaks on interannual time scales. However, neither reanalysis nor any model output show significant peaks on quasi-decadal time scales, with the possible exceptions of HadGEM3-GC31-LL (Fig. 4.5l) and MIROC6 (Fig. 4.5k). Because the SSTa pattern associated with the evolution of the PDP from Fig. 4.1e varies on the same time scale as the PDP, the results here suggest that the PDP is likely not related to variations in canonical ENSO.

Unlike the power spectrum analysis for the canonical ENSO time series for HadISST shown in Fig. 4.5a, the power spectrum analysis for CP ENSO shown in Fig. 4.6a has significant power on quasi-decadal time scales using *a priori* statistics. These results

are expected, as Furtado et al. (2012) and others have shown CP ENSO to have power on the decadal time scale. Juxtaposed with reanalysis are the results for model output (Fig. 4.6b-l). Models generally show power for their respective CP ENSO patterns at higher frequencies than shown in reanalysis. For example, ACCESS-CM2 and BCC-ESM1 (Fig. 4.6c,e) have peaks at ~2-3 years and CESM2-WACCM (Fig. 4.6h) has a peak at ~7 years. CESM2, UKESM1-0-LL, GISS-E2-1-G, and HadGEM3-GC31-LL (Fig. 4.6b,f,i,k) have significant peaks at quasi-decadal frequencies, but these are not as robust nor as broad as the peak shown in reanalysis. Overall, the evidence here shows that models used in this study do not simulate their respective CP ENSO structures with the same periodicity as found in reanalysis. However, the significant quasi-decadal peak in Fig. 4.6a is promising in that it shows CP ENSO in reanalysis has power on the same time scale as the PDP.

Comparing the spatial patterns and temporal variations in canonical ENSO and CP ENSO, while relevant, does not provide direct evidence that the PDP's Year 1 SSTa pattern is associated with these two modes; merely that they are similar. To quantitatively compare the SSTa pattern associated with the PDP to canonical and CP ENSO, a time series is created to represent the PDP's Year 1 SSTa pattern. This time series is created by spatially-averaging SSTa within a central Pacific domain (CP)(10°S - 10°N, 175°W - 130°W) and subtracting the spatially averaged SSTa in a western Pacific domain (WP) (0° - 20°N, 135°E - 150°E). The CP and WP domains were chosen as they largely encompass the statistically significant anomalies associated with the PDP's Year 1 SSTa pattern in the tropical Pacific. Fig. 4.2a shows the two domains overlaid on the regression of SSTa onto the PDP Index at lag Year 1 in reanalysis data.

The time series tracking the PDP's SSTa pattern and the time series for canonical and CP ENSO reanalysis data are subsequently filtered to isolate quasi-decadal variability and correlated with each other to determine how well they covary. The

resulting correlation for canonical ENSO and the PDP's SSTa pattern in reanalysis is weak ($r = 0.13$), while the time series tracking the SSTa pattern associated with the PDP correlates with the CP ENSO time series quite well ($r = 0.85$) and is highly significant ($p \ll 0.001$). The high correlation between the time series tracking the SSTa pattern associated with the PDP during the emergence of the N-S phase and the CP ENSO time series is robust evidence that the PDP and CP ENSO are indeed related.

Fig. 4.7 shows the filtered NDJFM CP ENSO time series for both reanalysis and model output correlated with the PDP index at various lags. The lag correlation plot for reanalysis (Fig. 4.7a) confirms that the emergence of the N-S phase of the PDP corresponds with CP ENSO in HadISST, as the two are significantly correlated at lags 0, 1 and 2 years (Fig. 3.6,4.7). Further, the significant negative correlations at lags -5 and -4 correspond with the evolution of cooler central Pacific SST seen in Anderson et al. (2016a) and Anderson et al. (2017). Taken together, these results demonstrate that the warming and cooling patterns associated with the evolution of the PDP in the tropical Pacific are indeed related to CP ENSO events in reanalysis.

In contrast to reanalysis, models show little evidence of any relationship between CP ENSO and the PDP index, with few models having correlations greater than a value of 0.2. The only model showing some consistent periodicity in its lag correlations is CESM2-WACCM (Fig. 4.7h). Yet, it is out of phase with reanalysis such that it shows negative lag correlations when reanalysis suggests a positive correlation. Overall, the model results from Fig. 4.7b-l further highlight how models struggle to simulate the relationship between the PDP and SSTa in the tropical Pacific existing in reanalysis data (Fig. 4.7).

The hypothesis proposed by Anderson et al. (2016a) for the maintenance of the N-S phase of the PDP is substantiated by the findings within the previous sections,

but only partially. In order to fully satisfy the hypothesis that the N-S phase of the PDP is partially driven by CP SST, it must be shown that:

1. CP SST varies on the same time scale and is in phase with the emergence of the N-S phase of the PDP

2. The CP SST associated with the PDP teleconnect to the extratropics, thereby influencing the atmospheric circulation in the North Pacific

The previous two sections have provided robust evidence that CP SST varies on the same time scale and that these variations are in phase with the emergence of the N-S phase of the PDP. The following section will outline a preliminary exploration of whether the CP SST associated with the PDP during the emergence of the N-S phase truly drives the transition to the N-S phase.

4.3   Dynamical Response to SSTa in the Tropics

The mechanism through which Anderson et al. (2016a) hypothesizes the PDP to be linked to CP SST is the atmospheric bridge, a phenomena which was briefly discussed in Chapter 1. In essence, variations in the longitudinal location of diabatic heating in the tropics can induce different Rossby wave patterns which subsequently modulate atmospheric circulation in the tropics. The following analysis investigates how the atmosphere responds to the SSTa pattern associated with the PDP at Year 1 in both reanalysis and models.

Recall the SSTa pattern associated with the evolution of the PDP at year 1 and the time series created to track it (Fig. 4.2a). Figure 4.8 shows SSTa in the tropical Pacific regressed onto this time series for both reanalysis and model data. The regression of SSTa in the tropical Pacific onto this the time series tracking this pattern recreates a similar one (Fig. 4.8a). Models tend to capture the same general pattern (Figs. 4.8b-l), with spatial correlations ranging from $r = 0.88$ for BCC-CSM2-MR (Fig. 4.8e) to

$r = 0.95$ for HadGEM3-GC31-LL (Fig. 4.8k). While the spatial correlations are high, there is some slight variation in the location of maximum positive anomalies with some models simulating it farther west (CESM2,CESM2-WACCM) and some simulating it farther east (GISS-E2-1-G,HadGEM3-GC31-LL). In general, the magnitude of the warm SSTa in models is considerably larger than reanalysis, especially for GISS-E2-1-G and CESM2 (Figs. 4.8b,i). The SSTa magnitudes shown here are consistent with the larger maximum variability in model simulations of both canonical ENSO (Fig. 4.3) and CP ENSO (Fig. 4.4). Moreover, cooler SSTa that are confined to the western Pacific are weaker than reanalysis in models, with CESM2, CESM2-WACCM, and ACCESS-CM2 being the exceptions (Figs. 4.8a,b,c,h). Model biases in the climatological state of the tropical Pacific may play a role in these particular patterns and will need to be investigated. The varying location and magnitude of the SSTa in Fig. 4.8 for model output, in addition to the variations in dominant time scales for canonical ENSO and CP ENSO (Figs. 4.3 and 4.4), imply that model ocean dynamics in the tropical Pacific are inconsistent with reanalysis. The subsequent atmospheric response to the lower tropospheric heating associated with this pattern of SSTa will therefore be different, changing the associated atmospheric patterns.

Next, to determine how similar the model atmospheric response is to reanalysis for the SSTa pattern in Fig. 4.8, 7-20 year^{-1} band-pass filtered 500 hPa eddy geopotential height anomalies are regressed onto the filtered lag Year 1 SSTa time series. Figure 4.9a shows the results of this regression for reanalysis, with Figs. 4.9b-l showing results for CMIP6 model output. For reanalysis, there is a meridional dipole in eddy geopotential height anomalies in the North Pacific that resembles the N-S phase of the PDP associated with variations in the time series tracking the SSTa pattern for the PDP at Year 1. In contrast to reanalysis, the results from CMIP6 model output vary considerably in their atmospheric responses to SSTa changes in the central and western Pacific (Figs. 4.9b-l). Overall, model teleconnection patterns appear to map

more onto the Pacific-North American (PNA) pattern as opposed to the N-S phase of the PDP as shown in reanalysis (Horel and Wallace, 1981; Wallace and Gutzler, 1981). Moreover, no spatial correlation between any model and reanalysis exceeds $r = 0.6$. The large variations in the simulated wave trains for model output with respect to reanalysis suggests that the atmospheric dynamics in models are not representative of those in observations on the decadal time scale. Interestingly, the results here demonstrate that CMIP6 models also struggle with similar biases to models used in the IPCC AR4. As shown by Furtado et al. (2011), models from IPCC AR4 failed to capture a connection between central tropical Pacific SST and the NPO. Figs. 4.9b-l shows similar results, with models demonstrating a teleconnection pattern that is more associated with canonical ENSO in observations than CP ENSO. The results here highlight a continuation of the inability of models to accurately capture the connection between the central tropical Pacific and the North Pacific on the quasi-decadal time scale.

4.4   Chapter Summary & Discussion

This chapter showed that the SSTa pattern observed within the tropical Pacific during the emergence of the N-S phase of the PDP is indeed related to tropical PDV, and specifically quasi-decadal variations in CP ENSO. This finding was supported by the spatial pattern of SSTa resembling the structure of CP ENSO (Fig. 4.4a), CP ENSO having power on the quasi-decadal time scale (Fig. 4.6a), and the time series' for the PDP's SSTa pattern and CP ENSO correlating well ($r = 0.85, p \ll 0.001$). In contrast, the SSTa pattern at Year 1 in the PDP's evolution does not relate to canonical ENSO well, despite the PDP's pattern indicating warm SSTa in the eastern Pacific as well (Fig. 4.1e), which indicates that the PDP is not related to the leading mode of variability in tropical Pacific SST. Additionally, investigating how the atmosphere responds to the SSTa pattern observed during the emergence of

the N-S phase of the PDP indicated that the SSTa pattern at Year 1 in the PDP's evolution also projects onto the N-S phase of the PDP. Though evidence of a direct dynamical link still needs to be explored, it is likely that decadal variations in CP SSTa play a role in the maintenance of the N-S phase of the PDP given these results. The implications of the findings within this chapter serve to further justify that the secondary mode framework for Pacific variability should also include the PDP, as the PDP is both related to the NPO and CP ENSO.

Unlike reanalysis, models tend to capture more of a PNA-like teleconnection pattern as a response to SSTa variations in the same region, which is more indicative of teleconnections from canonical ENSO than CP ENSO (Wallace and Gutzler, 1981; Furtado et al., 2012). A potential reason for this could be how models represent the mean states of both the atmosphere and ocean in the Pacific basin. Further research will need to address biases such as this to identify why models simulate an atmospheric response that varies considerably from reanalysis. Regardless of the reason, the inability of models to recreate the same teleconnection pattern seen in reanalysis likely plays a role in how they simulate the emergence maintenance of the N-S phase of the PDP. The implications for the inaccuracy of model teleconnection patterns on the quasi-decadal timescale are important, as different teleconnection patterns have different impacts on North Pacific and North American climate. Were the models within this study to be used for predictions and decadal climate projections, the patterns shown in Figs. 4.9b-l would likely lead to a much different forecast for North American given that the PNA pattern has been connected to regional temperature and precipitation patterns in different locations across North American than the NPO (Leathers et al., 1991; Baxter and Nigam, 2015).

In their analysis on the PDP, Anderson et al. (2017) proposed a possible reason for models not capturing the SSTa pattern observed during the emergence of the N-S phase of the PDP in reanalysis for CCSM4 output: models may lack equatorward

transport of subsurface temperature anomalies, something akin to the North Pacific Meridional Mode (NPMM; Vimont et al., 2003; Chiang and Vimont, 2004). Anderson et al. (2017) briefly discussed the lack of equatorward transport of subsurface temperature anomalies in CCSM4 and how it might hinder models' ability to simulate the transition from the E-W phase of the PDP back to the N-S phase. They found that while reanalysis showed significant subsurface temperature anomalies in the eastern subtropical Pacific, CCSM4 did not replicate this. The equatorward transport of these anomalies is a well-established pathway through which the extratropics can inject variance into the tropics (Amaya et al., 2019). Indeed, both subsurface temperature and zonal wind stress anomalies within this region, which can be forced in part by modification of wind stress fields in the Pacific by the NPO (Penland and Sardeshmukh, 1995), have been linked to initiating ENSO and CP ENSO events (the "Seasonal Footprinting Mechanism"; Vimont et al., 2001, 2003). The inability of models to replicate the influence of the extratropics on ENSO initiation remains a potential explanation for how they misrepresent CP ENSO spatially and temporally. Future studies should identify the role of the NPMM in the initiation of the SSTa pattern associated with the emergence of the N-S phase of the PDP and subsequently compare this to model output to determine how model simulations of the NPMM impact their simulation of the PDP.
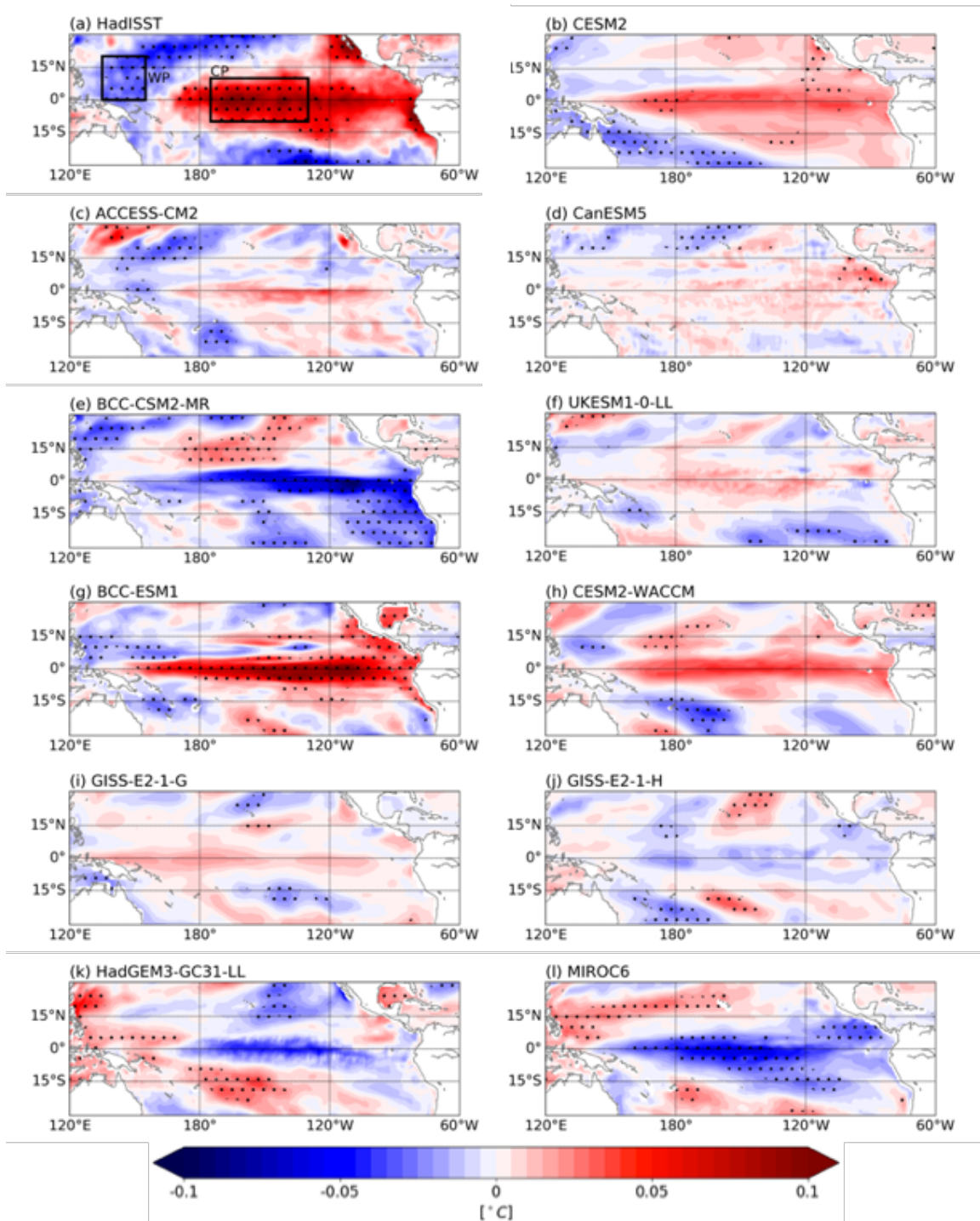
Figure 4.2: Regression of NDJFM averaged monthly mean SSTa ($^{\circ}C$) in the tropical Pacific onto the PDP Index at a lag of 1 year (PDP Index leads SSTa) for **(a)** HadISST and **(b-l)** select CMIP6 models. Stippling indicates statistically significant regression coefficients at the 95% confidence level using a bootstrapping method with 5000 iterations.
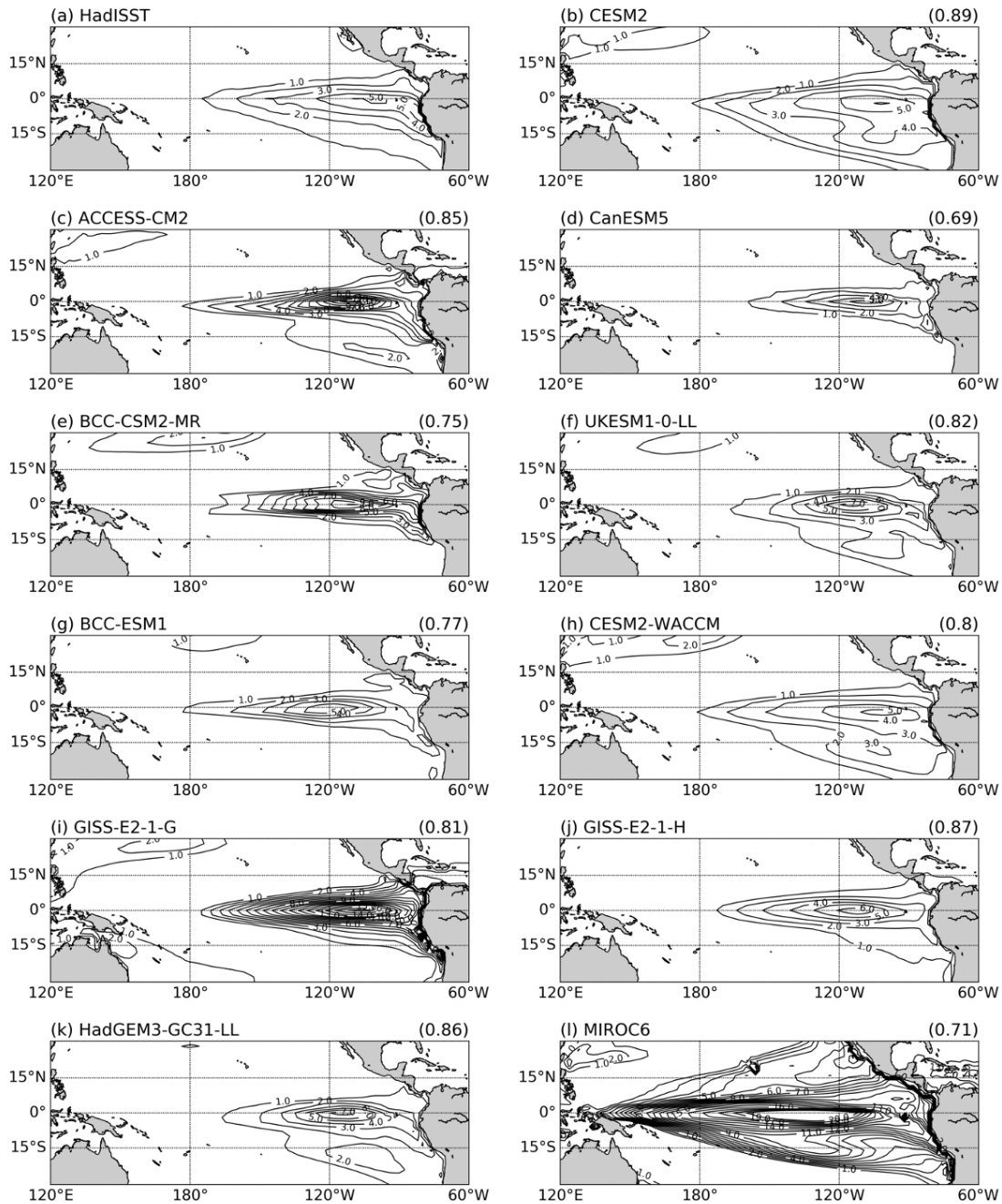
Figure 4.3: **(a)** Standard deviation of the leading EOF in tropical Pacific SSTa after removing variability associated with the Niño4 index at lags -3 to +3 months via multi-linear regression for HadISST from 1870-2014 over the domain 30°S - 30°N, 120°E-60°W. **(b-l)** same as **(a)** but for a 300 year of preindustrial control run of each respective model. Values included in parenthesis are the spatial correlations of each model with HadISST results shown in **(a)**.
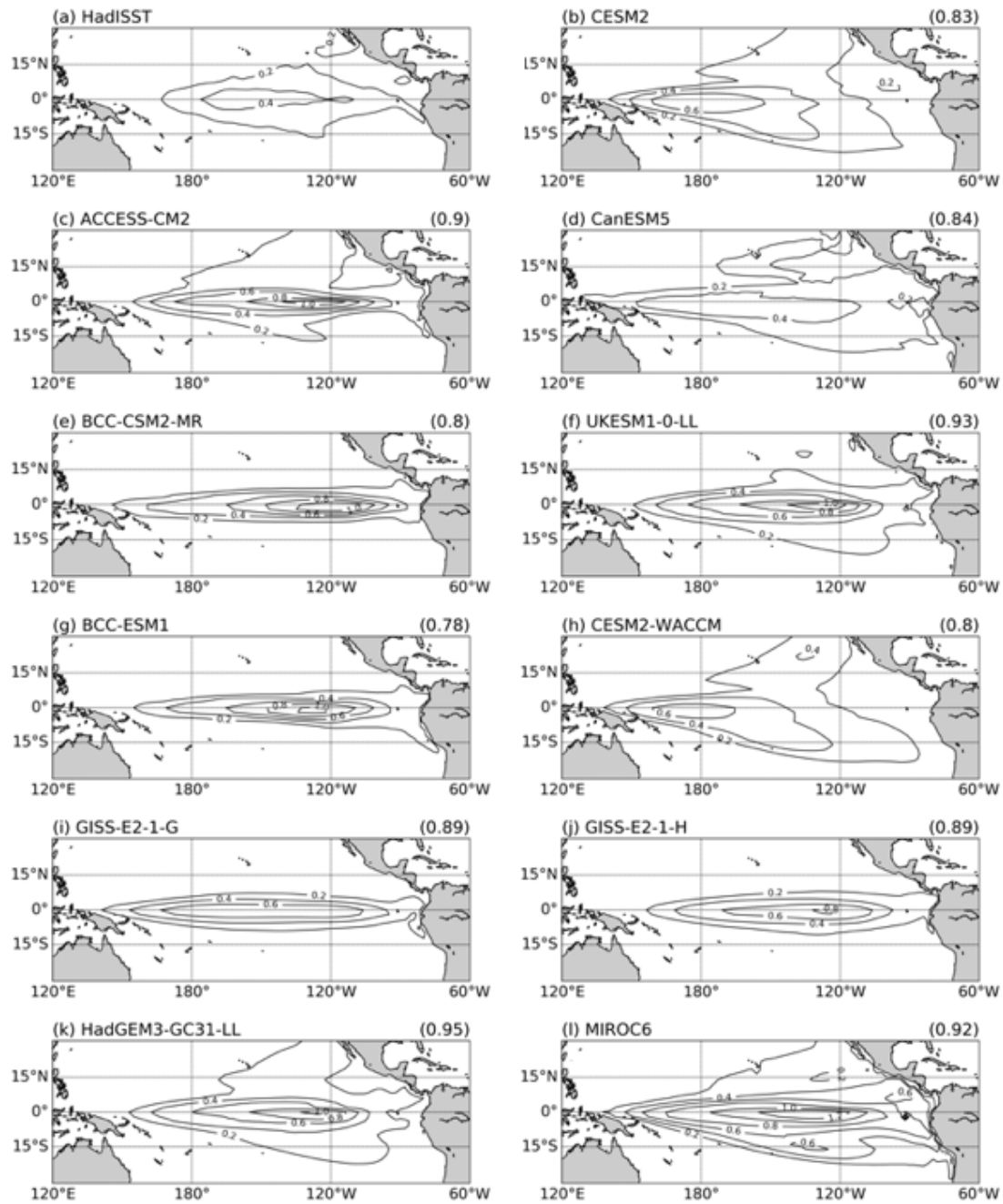
Figure 4.4: **(a)** CP ENSO structure in HadISST (1870-2014) **(b-l)** same as **(a)** but for a 300 year of preindustrial control run of each respective model. Values included in parenthesis are the spatial correlations of each model with HadISST results shown in **(a)**.
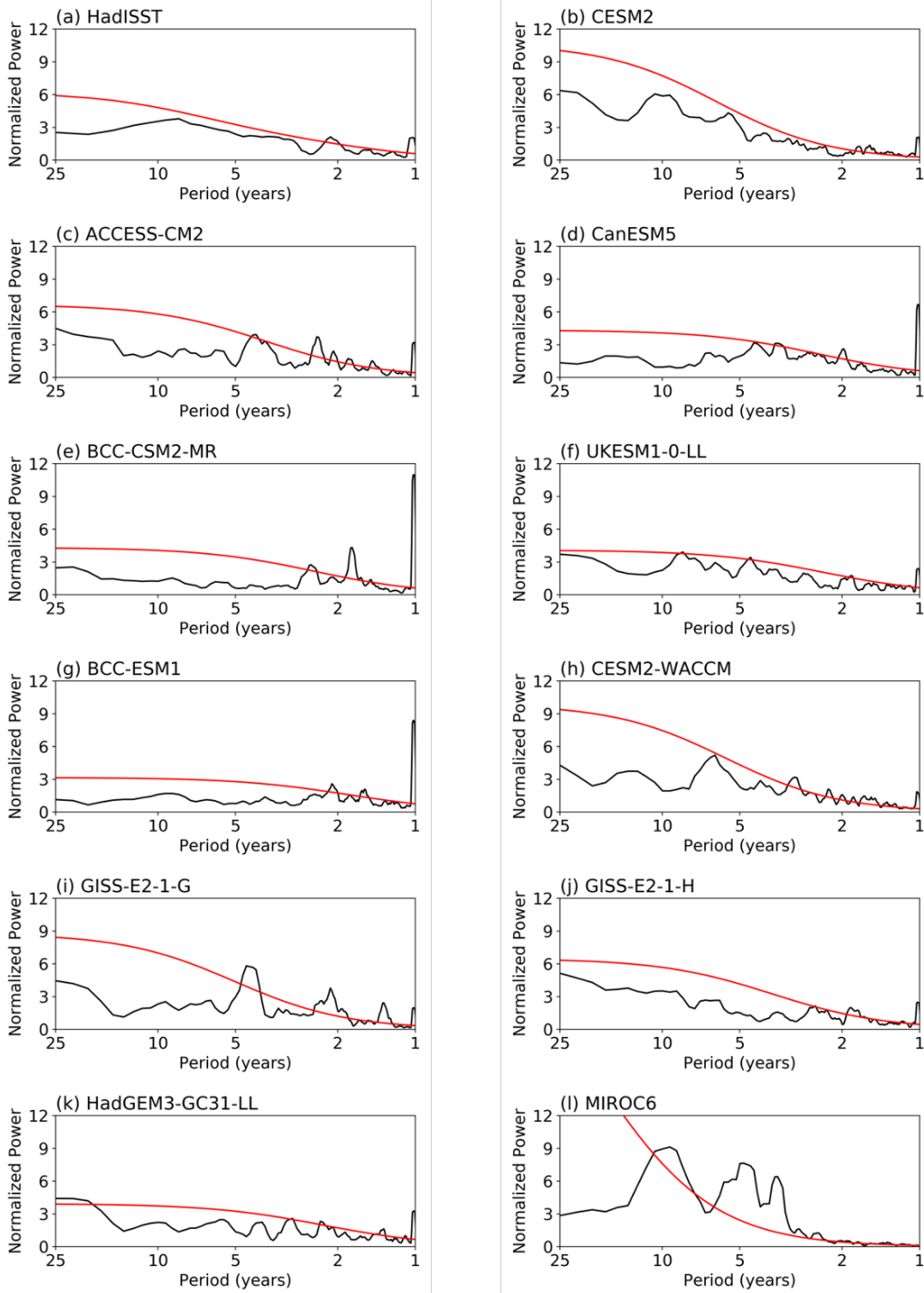
Figure 4.5: Power spectrum analysis on the time series associated with each of the canonical ENSO patterns from Fig. 4.3 for **(a)** HadISST and **(b-l)** CMIP6 model output. The 95% confidence spectrum using *a priori* statistics is plotted in red.
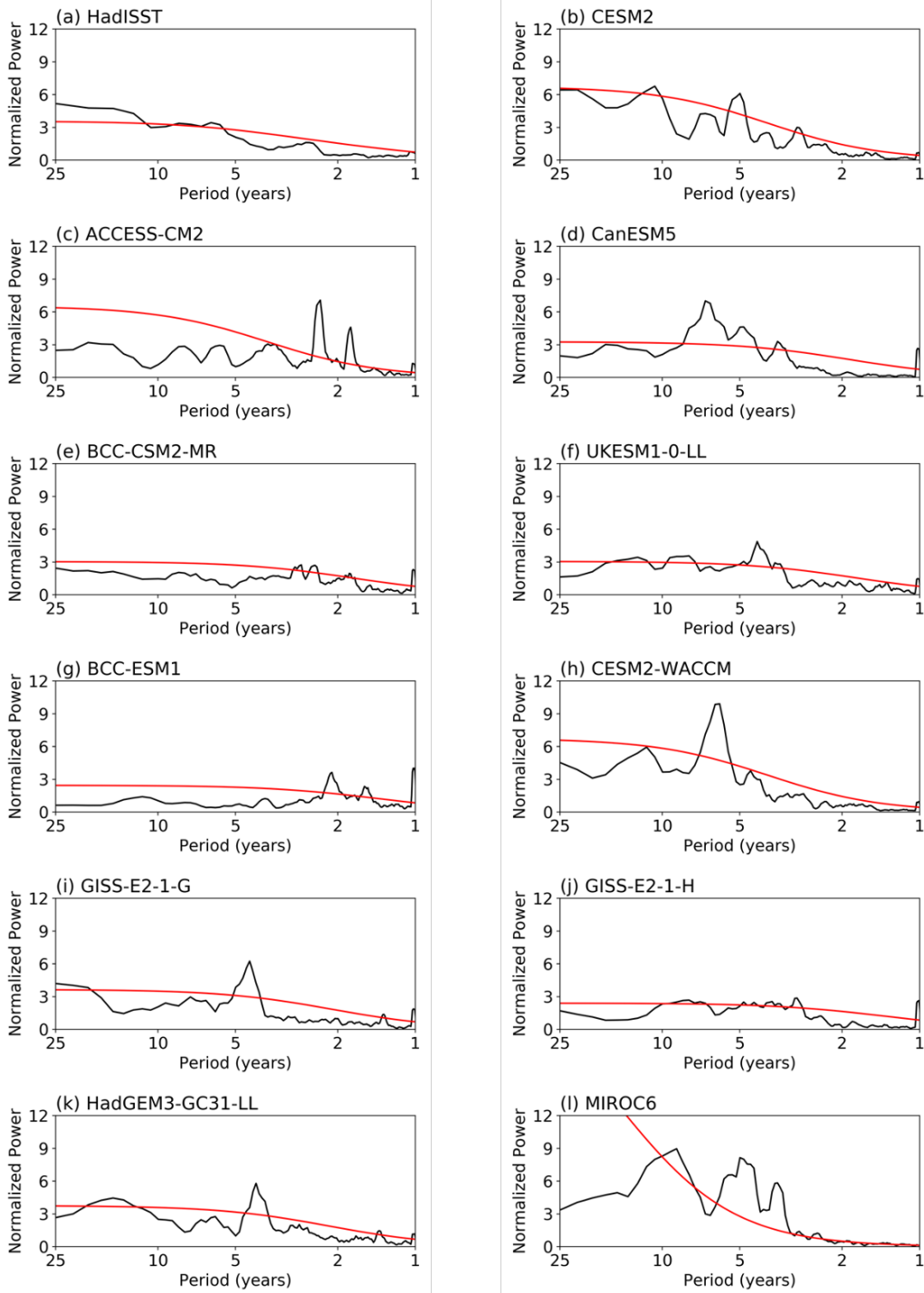
Figure 4.6: Power spectrum analysis on the time series associated with each of the CP ENSO patterns from Fig. 4.4 for **(a)** HadISST and **(b-l)** CMIP6 model output. The 95% confidence spectrum using *a priori* statistics is plotted in red.
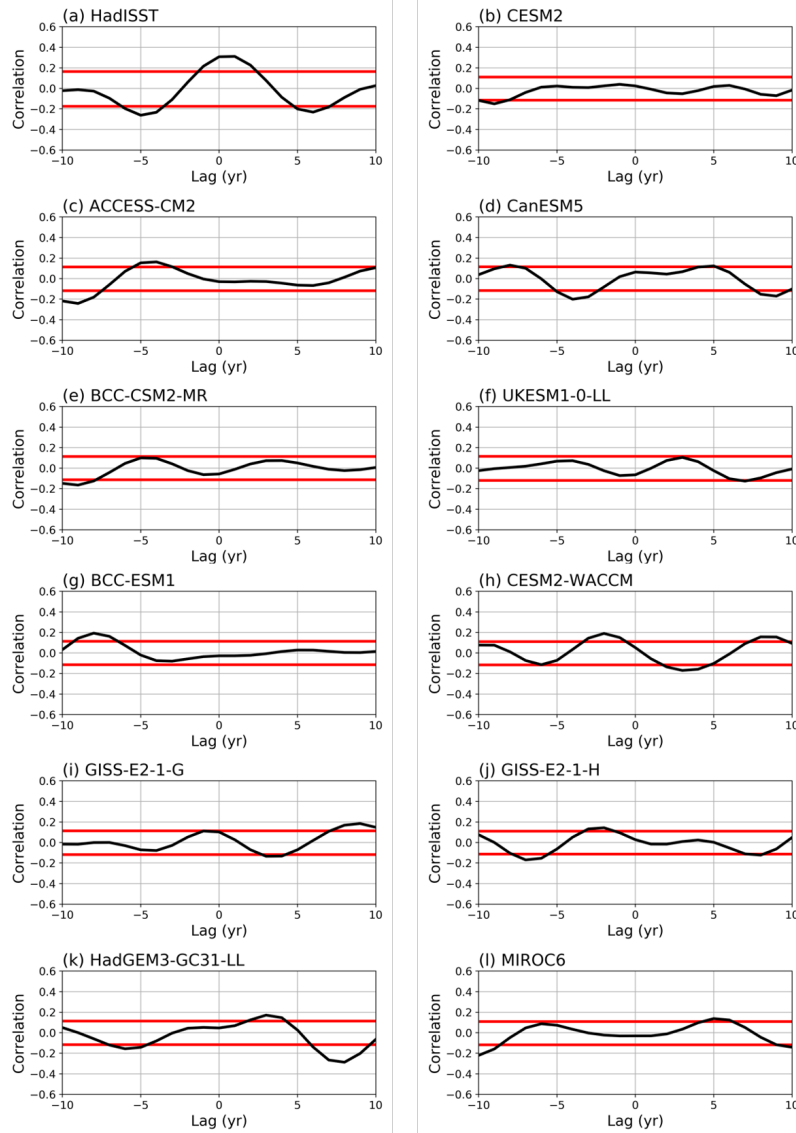
Figure 4.7: Lag correlation plots at lag -10 to +10 years of the PDP Index and the 7-20 year^{-1} band-passed NDJFM-averaged CP ENSO index. Negative (positive) lags mean the PDP lags (leads) the CP ENSO index.**(a)** HadISST Central Pacific ENSO time series is correlated with the PDP Index from the 20th Century Reanalysis (1870-2014).**(b-l)** The same, but for the first 300 years of output from preindustrial control runs. The 95% confidence interval through use of a two-sided bootstrapping method with 5000 iterations is shown in red.
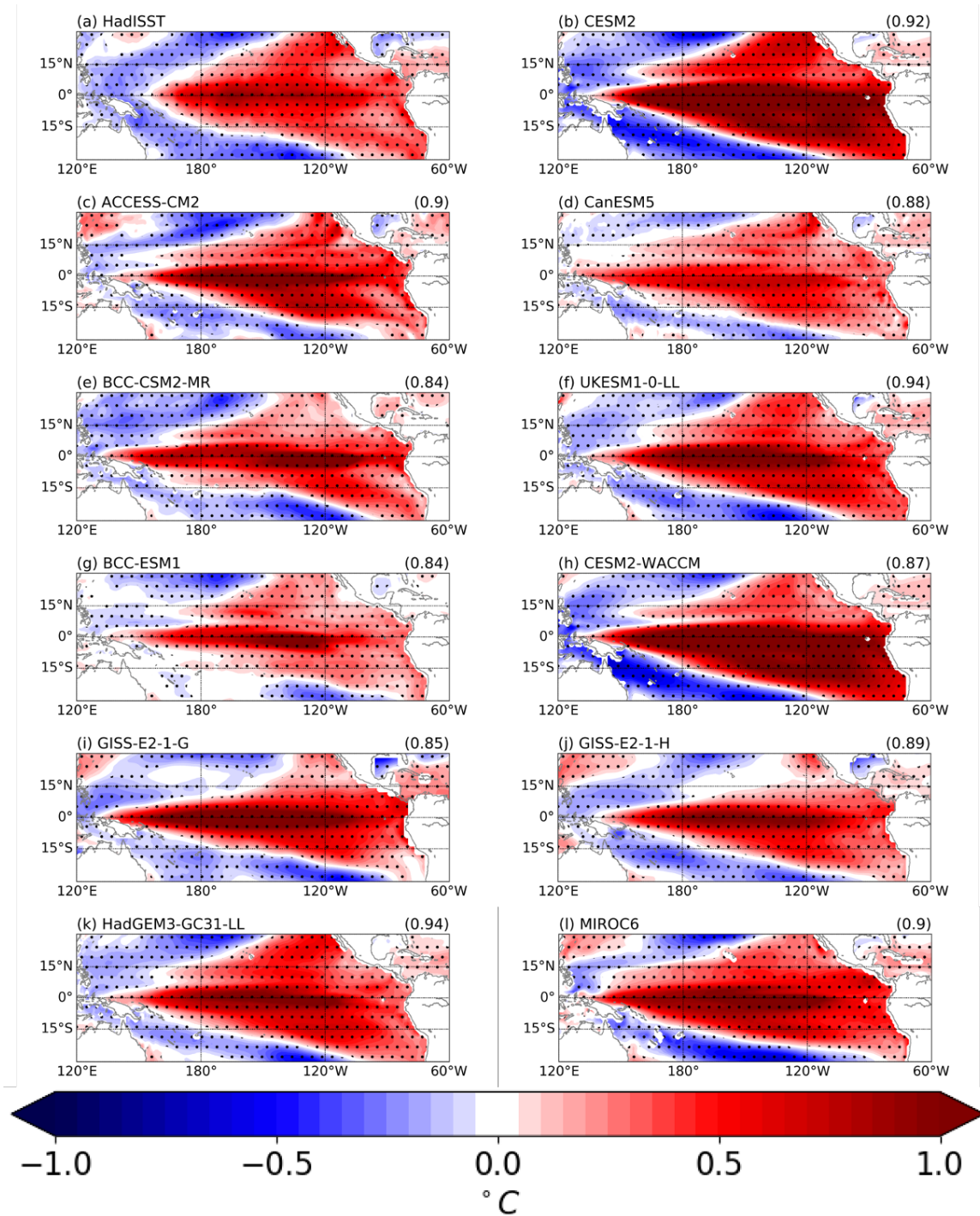
Figure 4.8: Regression of NDJFM averaged monthly mean SSTa ($°C$) onto the ND-JFM averaged time series created to track the Year 1 SSTa pattern associated with the PDP for **(a)** HadISST and **(b-l)** CMIP6 model output. Stippling indicates statistical significance using a bootstrapping method with 5000 iterations at the 95% confidence level.
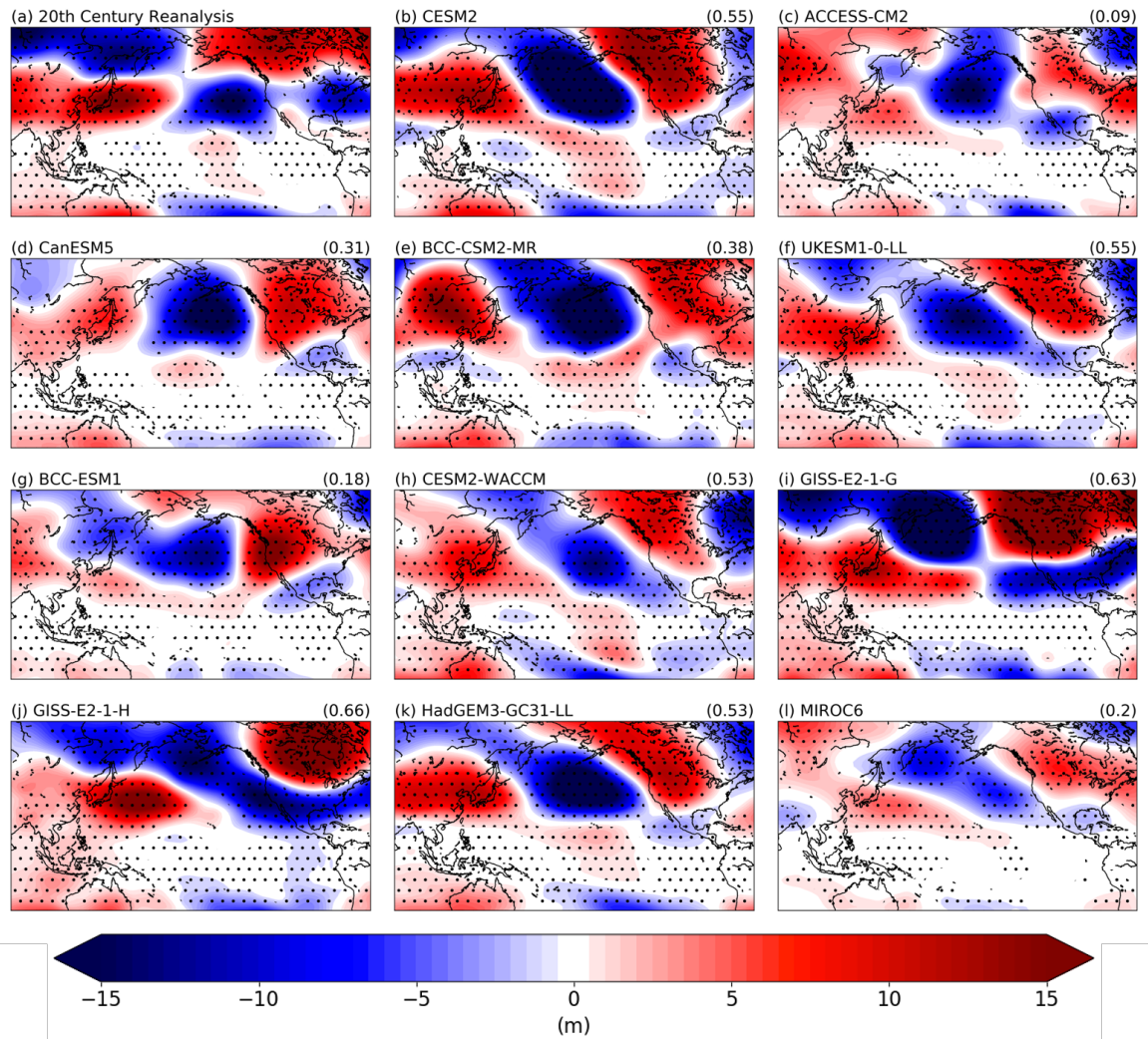
Figure 4.9: Regression of 7-20 year^{-1} band-pass filtered NDJFM averaged monthly-mean eddy geopotential height anomalies (m) onto the standardized NDJFM averaged monthly mean time series tracking the Year 1 SSTa pattern for the PDP for **(a)** HadISST and **(b-f)** CMIP6 model output. Stippling indicates statistical significance using a bootstrapping method with 5000 iterations at the 95% confidence level.

Chapter 5

Summary and Discussion

This thesis investigated relationships between the N-S phase of the PDP, the NPO, and SSTa in the central tropical Pacific in both reanalysis and CMIP6 model output. Findings show that the PDP is directly related to fluctuations in the NPO in reanalysis. The relationship between the N-S phase of the PDP and the NPO is evidenced by the filtered NPO index explaining ∼45% of the variance in the PDP index (Fig. 3.4) and lag-regressions of filtered 850 hPa geopotential height anomalies onto the NPO index, effectively recreating the evolution of the PDP (Fig. 3.5). However, a large portion of the variance in the PDP index is not explained by the NPO index (∼55%) which is likely due to the NPO index not capturing variability associated with the E-W phase of the PDP. While these results support the inference from Anderson et al. (2017) that the N-S phase of the PDP maps onto the NPO, they also reaffirm the importance of differentiating the N-S phase and the E-W phase of the PDP, especially dynamically.

This study also demonstrated a relationship between the N-S phase of the PDP and tropical Pacific climate variability. Several key analyses established this relationship. The SSTa pattern associated with the emergence of the N-S and phase of the PDP is similar the structure of CP ENSO in HadISST, with statistically significant anomalies situated in the central Pacific (Fig. 4.1). The CP ENSO time series derived for HadISST had significant power at quasi-decadal frequencies (Fig. 4.6), was highly correlated with the time series describing the PDP SSTa pattern at lag Year +1 ($r = 0.85, p \ll 0.001$), and is significantly correlated with the PDP index when lagged by one year (Fig. 4.7). Much of the same analysis was conducted with canonical ENSO, and no significant relationship was found with the SSTa pattern

associated with the emergence of the N-S phase of the PDP. The canonical ENSO structure in reanalysis varies from the observed SSTa pattern associated with the PDP at Year 1 (Fig. 4.3a), has little power at quasi-decadal frequencies (Fig. 4.5a), and is weakly correlated with the time series describing the SSTa pattern associated with the PDP during the emergence of the N-S phase ($r = 0.13, p \ll 0.001$) Based on these results, low frequency variations in CP ENSO are indeed related to the N-S phase of the PDP, much more so than canonical ENSO.

Recall the hypotheses proposed for this thesis:

1) The N-S phase of the PDP is intimately tied to variability in the NPO.

2) The N-S phase of the PDP is linked to tropical PDV.

3) AOGCMs capture show evidence of relationships between the N-S phase of the PDP, the NPO, and tropical PDV.

The results in this thesis demonstrate that the N-S phase is intimately tied to variability in the NPO and that the emergence of the N-S phase of the PDP is linked to tropical PDV. Synthesizing these relationships results in a robust argument to include the PDP within the secondary mode paradigm for Pacific variability. Just how the PDP is placed within this paradigm, however, remains to be seen. Relationships between the PDP and other modes of variability in the Pacific will need to be researched to confidently place it within this paradigm. Another potential linkage to the PDP yet to be explored is the connections between the PDP and the NPGO. The secondary mode paradigm for North Pacific variability (i.e., CP ENSO-NPO-NPGO) establishes that the NPO forces some variability in the NPGO. With results here showing the N-S phase of the PDP mapping onto the NPO and and the concomitant SSTa evolution in the tropics being related to CP ENSO, there may be a linkage to the NPGO on the quasi-decadal time scale as well. Further, as shown by Frankignoul and Sennéchael (2007), SSTa in the North Pacific can substantially impact overlying

circulation which indicates that the NPGO may influence the evolution of the PDP as well. The intricacies of whether the PDP and NPGO relate to one another and, if so, to what extent they influence one another will need to explored in future studies.

Not investigated within this study is the second hypothesis presented by Anderson et al. (2017), which proposes that the E-W phase of the PDP is maintained by stratospheric temperature deviations and their effect on the underlying tropospheric circulation. As discussed in Chapter 1, this could be a lagged influence from tropical Pacific SST forcing on the stratosphere. Indeed, Domeisen et al. (2019) found that the state of the polar stratospheric vortex is profoundly affected by ENSO variability, with more sudden stratospheric warmings (SSWs; i.e., a reversal of wintertime westerly zonal-mean zonal winds at 10 hPa and 60° N) occurring during El Niño years. SSWs can have a strong impact on the underlying tropospheric circulation (Baldwin and Dunkerton, 1999; Baldwin et al., 2001) and may have decadal variability (van Loon and Labitzke, 2011). Future research needs to address if, and to what extent, influence from stratosphere on the troposphere impacts the evolution of the PDP and whether this can be traced to ENSO. The E-W phase of the PDP has large implications for decadal variability in seasonal precipitation in the Northwestern US (Anderson et al., 2016a), and further understanding of what drives the E-W phase can lead to the improvement of AOGCMs and more skilled predictions of drought/pluvial cycles in this region of the US.

Historically, AOGCMs have not performed well with replicating variability in the stratosphere (Charlton-Perez et al., 2013; Seviour et al., 2016). Many models require modes of variability within the stratosphere to be externally forced, if modes of variability in the stratosphere are simulated at all, as the stratospheric physics within current models is not complete (i.e., the Quasi-Biennial Oscillation; Anstey et al., 2016). If the hypothesis from Anderson et al. (2017) proposing that the E-W phase may be maintained by stratospheric influences on the troposphere is true,

models should be expected to struggle simulating this phase due to their lack of skill in simulating stratospheric variability. Indeed, Figures 3.6c,d showing CMIP6 model performance in simulating the E-W phase of the PDP is consistent with this hypothesis, as all models struggle in capturing a distinct E-W phase. Moreover, models with high tops (i.e., more resolution in the stratosphere) like CESM2-WACCM show no noticeable improvement in their simulation of the E-W phase within this study. Should the E-W phase of the PDP be forced in part by the stratosphere, further improvement of stratospheric resolution and dynamics will be crucial in improving predictions of this mode of variability.

Contrary to reanalysis, the model analyses within this study do not support the PDP playing a role in the secondary mode paradigm. Model results vary considerably from reanalysis both on their simulations of the PDP and on the connection between the N-S phase of the PDP and the NPO. Simulations of the PDP's relationship to Central Pacific SSTa at Year 1 in CMIP6 models is weak, with few showing statistically significant anomalies in the same region as in reanalysis and some showing anomalies of the wrong sign (Fig. 4.1,4.2). Models do not simulate tropical Pacific variability well, both spatially and temporally, as shown by their CP ENSO structure (Fig. 4.4) and the power spectra of CP ENSO time series (Fig. 4.6). Moreover, the connection between CP SST and the N-S phase of the PDP is virtually non-existent in model output, as the atmospheric response to heating in the central Pacific does not map onto the N-S phase of the PDP like in reanalysis (Fig. 4.9) and appears to map more on the AL. The findings here generally show that all models struggle with simulating North PDV and highlight a continuation of discrepancies in how IPCC AR4 models simulated North PDV as shown by Furtado et al. (2011), now with respect to the PDP.

Current climate projections for the North Pacific and across North America are primarily informed by variability associated with the leading modes of Pacific variability (i.e., the ENSO-AL-PDO paradigm). Yet, exclusively using this paradigm does not capture necessary variability to explain events in the North Pacific and across North America, such as extreme cold in the midwestern United States during the winter of 2013/14 (Baxter and Nigam, 2015). For the PDP specifically, research currently being conducted by the authors of Anderson et al. (2017) shows that the phase of the PDP has a stronger connection to surface temperature and precipitation extremes over North America than the leading mode of atmospheric variability in the North Pacific (i.e., the AL). As such, the inclusion of variability in the secondary mode paradigm, including the PDP, can improve subseasonal-to-seasonal (S2S) forecasts for surface temperature and precipitation extremes. However, prior to the inclusion of the PDP within climate predictions, our current understanding of the PDP's dynamics and model performance in simulating these dynamics need to be improved. Identifying observed oceanic or atmospheric features AOGCMs struggle with simulating can, and has in the case of the Madden-Julian Oscillation (Zhang, 2005), aid in improving their dynamics and thereby improve prediction skill. For quasi-decadal variability specifically, Liu and Di Lorenzo (2018) discuss in their review that PDV is primarily driven by teleconnection dynamics interacting with the tropics and between ENSO teleconnections and modes of atmospheric variability in mid-latitudes. The results from this study show that CMIP6 models do not capture tropical PDV (Fig. 4.4,4.6) nor the teleconnection dynamics associated with PDV (Fig. 4.9). Because of this, models are not able to capture the relationship between tropical Pacific and the PDP, thereby hindering their simulations of the PDP's evolution and associated impacts. Improving how models simulate the dynamical drivers of the PDP demonstrated in this study will thus be crucial for forecasting PDP-related impacts like drought/pluvial cycles

and extreme temperatures across the US across time scales ranging from subseasonal to decadal.

Finally, the link demonstrated within this study between the emergence of the N-S phase of the PDP and tropical PDV requires further research. While the atmospheric response to the SSTa pattern associated with the emergence of the N-S phase of the PDP maps onto the N-S phase (Fig. 4.9), it is still unclear just how much this contributes to the emergence of the N-S phase of the PDP. Future research, informed by the performance of CMIP6 models in simulating tropical PDV and the PDP detailed in this study, will need to confirm this. Much like methods seen in Amaya et al. (2019), future studies should select a model and force the pattern of SSTa associated with the PDP in an ensemble of model runs in order to quantify the dynamical link between CP SST and the N-S phase of the PDP. Should the relationship between tropical PDV and the north-south phase of the PDP prove to be both dynamical and quantifiable, it could have implications for the improving predictability of the PDP and it's impacts in the North Pacific and across North America. Furthermore, with increasing variance in CP ENSO under anthropogenic climate change (Yeh et al., 2009), establishing a better understanding of how tropical PDV influences the PDP is all the more important to improve prediction skill.

Bibliography

Alexander, M. A., I. Bladé, M. Newman, J. R. Lanzante, N.-C. Lau, and J. D. Scott, 2002: The Atmospheric Bridge: The Influence of ENSO Teleconnections on Air–Sea Interaction over the Global Oceans. *Journal of Climate*, **15 (16)**, 2205–2231, doi:10.1175/1520-0442(2002)015⟨2205:TABTIO⟩2.0.CO;2.

Amaya, D. J., Y. Kosaka, W. Zhou, Y. Zhang, S. P. Xie, and A. J. Miller, 2019: The North Pacific Pacemaker Effect on Historical ENSO and its Mechanisms. *Journal of Climate*, **32 (22)**, 7643–7661, doi:10.1175/JCLI-D-19-0040.1.

Anderson, B. T., J. C. Furtado, E. Di Lorenzo, and D. J. Short Gianotti, 2017: Tracking the Pacific Decadal Precession. *Journal of Geophysical Research*, **122 (6)**, 3214–3227, doi:10.1002/2016JD025962.

Anderson, B. T., D. J. S. Gianotti, J. C. Furtado, and E. Di Lorenzo, 2016a: A Decadal Precession of Atmospheric Pressures over the North Pacific. *Geophysical Research Letters*, **43 (8)**, 3921–3927, doi:10.1002/2016GL068206.

Anderson, B. T., D. J. S. Gianotti, G. Salvucci, and J. Furtado, 2016b: Dominant Time Scales of Potentially Predictable Precipitation Variations across the Continental United States. *Journal of Climate*, **29 (24)**, 8881–8897, doi:10.1175/JCLI-D-15-0635.1.

Anstey, J. A., J. F. Scinocca, and M. Keller, 2016: Simulating the QBO in an Atmospheric General Circulation Model: Sensitivity to Resolved and Parameterized Forcing. *Journal of the Atmospheric Sciences*, **73 (4)**, 1649–1665, doi:10.1175/JAS-D-15-0099.1.

Ashok, K., S. K. Behera, S. A. Rao, H. Weng, and T. Yamagata, 2007: El Niño Modoki and its possible teleconnection. *Journal of Geophysical Research: Oceans*, **112 (11)**, 1–27, doi:10.1029/2006JC003798.

Baldwin, M. P. and T. J. Dunkerton, 1999: Propagation of the Arctic Oscillation from the stratosphere to the troposphere. *Journal of Geophysical Research Atmospheres*, **104 (D24)**, 30 937–30 946, doi:10.1029/1999JD900445.

Baldwin, M. P., et al., 2001: The Quasi-Biennial Oscillation. *Reviews of Geophysics*, **39 (2)**, 179–229, doi:10.1029/1999RG000073.

Barlow, M., S. Nigam, and E. H. Berbery, 2001: ENSO, Pacific Decadal Variability, and U.S. Summertime Precipitation, Drought, and Stream Flow. *Journal of Climate*, **14 (9)**, 2105–2128, doi:10.1175/1520-0442(2001)014⟨2105:EPDVAU⟩2.0.CO;2.

Barnston, A. G. and R. E. Livezey, 1987: Classification, Seasonality and Persistence of Low-Frequency Atmospheric Circulation Patterns. *Monthly Weather Review*, **115 (6)**, 1083–1126, doi:10.1175/1520-0493(1987)115⟨1083:CSAPOL⟩2.0.CO;2.

Barsugli, J. J. and P. D. Sardeshmukh, 2002: Global Atmospheric Sensitivity to Tropical SST Anomalies throughout the Indo-Pacific Basin. *Journal of Climate*, **15 (23)**, 3427–3442, doi:10.1175/1520-0442(2002)015⟨3427:GASTTS⟩2.0.CO;2.

Baxter, S. and S. Nigam, 2015: Key role of the North Pacific Oscillation–West Pacific Pattern in Generating the Extreme 2013/14 North American Winter. *Journal of Climate*, **28 (20)**, 8109–8117, doi:10.1175/JCLI-D-14-00726.1.

Bjerknes, J., 1959: Monthly Weather Reyiew Atmospheric Teleconnections From the Equatorial Pacific. *Monthly Weather Review*, **97 (3)**, 163–172, doi:10.1175/1520-0493(1969)097⟨0163:ATFTEP⟩2.3.CO;2.

Bond, N. A., M. F. Cronin, H. Freeland, and N. Mantua, 2015: Causes and impacts of the 2014 warm anomaly in the NE Pacific. *Geophysical Research Letters*, **42 (9)**, 3414–3420, doi:10.1002/2015GL063306.

Bond, N. A., J. E. Overland, M. Spillane, and P. Stabeno, 2003: Recent shifts in the state of the North Pacific. *Geophysical Research Letters*, **30 (23)**, 2183, doi:10.1029/2003GL018597.

Capotondi, A., P. D. Sardeshmukh, and L. Ricciardulli, 2018: The Nature of the Stochastic Wind Forcing of ENSO. *Journal of Climate*, **31 (19)**, 8081–8099, doi:10.1175/JCLI-D-17-0842.1.

Charlton-Perez, A. J., et al., 2013: On the lack of stratospheric dynamical variability in low-top versions of the CMIP5 models. *Journal of Geophysical Research: Atmospheres*, **118 (6)**, 2494–2505, doi:10.1002/jgrd.50125.

Chiang, J. C. and D. J. Vimont, 2004: Analogous Pacific and Atlantic Meridional Modes of Tropical Atmosphere-Ocean Variability. *Journal of Climate*, **17 (21)**, 4143–4158, doi:10.1175/JCLI4953.1.

Chu, C., H. Hu, X.-Q. Yang, and D. Yang, 2020: Midlatitude atmospheric transient eddy feedbacks influenced ENSO-associated wintertime Pacific teleconnection patterns in two PDO phases. *Climate Dynamics*, **54 (3-4)**, 2577–2595, doi:10.1007/s00382-020-05134-4.

Compo, G. P., et al., 2011: The Twentieth Century Reanalysis Project. *Quarterly Journal of the Royal Meteorological Society*, **137 (654)**, 1–28, doi:10.1002/qj.776.

Danabasoglu, G., 2019: NCAR CESM2-WACCM model output prepared for CMIP6 CMIP piControl. Earth System Grid Federation, doi:10.22033/ESGF/CMIP6.10094.

Danabasoglu, G., D. Lawrence, K. Lindsay, W. Lipscomb, and G. Strand, 2019: NCAR CESM2 model output prepared for CMIP6 CMIP piControl. Earth System Grid Federation, doi:10.22033/ESGF/CMIP6.7733.

Deser, C., M. A. Alexander, and M. S. Timlin, 2003: Understanding the Persistence of Sea Surface Temperature Anomalies in Midlatitudes. *Journal of Climate*, **16 (1)**, 57–72, doi:10.1175/1520-0442(2003)016⟨0057:UTPOSS⟩2.0.CO;2.

Deser, C., I. R. Simpson, K. A. McKinnon, and A. S. Phillips, 2017: The Northern Hemisphere Extratropical Atmospheric Circulation Response to ENSO: How Well Do We Know It and How Do We Evaluate Models Accordingly? *Journal of Climate*, **30 (13)**, 5059–5082, doi:10.1175/JCLI-D-16-0844.1.

Deser, C. and J. M. Wallace, 1990: Large-Scale Atmospheric Circulation Features of Warm and Cold Episodes in the Tropical Pacific. *Journal of Climate*, **3 (11)**, 1254–1281, doi:10.1175/1520-0442(1990)003⟨1254:LSACFO⟩2.0.CO;2.

Deser, C., et al., 2012: ENSO and Pacific Decadal Variability in the Community Climate System Model Version 4. *Journal of Climate*, **25 (8)**, 2622–2651, doi:10.1175/JCLI-D-11-00301.1.

Di Lorenzo, E., K. M. Cobb, J. C. Furtado, N. Schneider, B. T. Anderson, A. Bracco, M. A. Alexander, and D. J. Vimont, 2010: Central Pacific El Niño and decadal climate change in the North Pacific Ocean. *Nature Geoscience*, **3 (11)**, 762–765, doi:10.1038/ngeo984.

Di Lorenzo, E., G. Liguori, N. Schneider, J. C. Furtado, B. T. Anderson, and M. A. Alexander, 2015: ENSO and meridional modes: A null hypothesis for Pacific climate variability. *Geophysical Research Letters*, **42 (21)**, 9440–9448, doi:10.1002/2015GL066281.

Di Lorenzo, E. and N. Mantua, 2016: Multi-year persistence of the 2014/15 North Pacific marine heatwave. *Nature Climate Change*, **6 (11)**, 1042–1047, doi:10.1038/nclimate3082.

Di Lorenzo, E., et al., 2008: North Pacific Gyre Oscillation links ocean climate and ecosystem change. *Geophysical Research Letters*, **35 (8)**, L08 607, doi:10.1029/2007GL032838.

Di Lorenzo, E., et al., 2013: Synthesis of Pacific Ocean Climate and Ecosystem Dynamics. *Oceanography*, **26 (4)**, 68–81, doi:10.5670/oceanog.2013.76.

Diaz, H. F., M. P. Hoerling, and J. K. Eischeid, 2001: Enso variability, teleconnections and climate change. *International Journal of Climatology*, **21 (15)**, 1845–1862, doi:10.1002/joc.631.

Diffenbaugh, N. S., D. L. Swain, and D. Touma, 2015: Anthropogenic warming has increased drought risk in California. *Proceedings of the National Academy of Sciences*, **112 (13)**, 3931–3936, doi:10.1073/pnas.1422385112.

Dix, M., et al., 2019: CSIRO-ARCCSS ACCESS-CM2 model output prepared for CMIP6 CMIP piControl. Earth System Grid Federation, doi:10.22033/ESGF/CMIP6.4311.

Domeisen, D. I., C. I. Garfinkel, and A. H. Butler, 2019: The Teleconnection of El Niño Southern Oscillation to the Stratosphere. *Review of Geophysics*, **57 (1)**, 5–47, doi:10.1029/2018RG000596.

Duffy, P. A., J. E. Walsh, J. M. Graham, D. H. Mann, and T. S. Rupp, 2005: Impacts of Large-Scale Atmospheric–Ocean Variability on Alaskan Fire Season Severity. *Ecological Applications*, **15 (4)**, 1317–1330, doi:10.1890/04-0739.

Eyring, V., S. Bony, G. A. Meehl, C. A. Senior, B. Stevens, R. J. Stouffer, and K. E. Taylor, 2016: Overview of the Coupled Model Intercomparison Project Phase 6 (CMIP6) experimental design and organization. *Geoscientific Model Development*, **9 (5)**, 1937–1958, doi:10.5194/gmd-9-1937-2016.

Frankignoul, C. and N. Sennéchael, 2007: Observed Influence of North Pacific SST Anomalies on the Atmospheric Circulation. *Journal of Climate*, **20 (3)**, 592–606, doi:10.1175/JCLI4021.1.

Furtado, J. C., E. Di Lorenzo, B. T. Anderson, and N. Schneider, 2012: Linkages between the North Pacific Oscillation and central tropical Pacific SSTs at low frequencies. *Climate Dynamics*, **39 (12)**, 2833–2846, doi:10.1007/s00382-011-1245-4.

Furtado, J. C., E. Di Lorenzo, N. Schneider, and N. A. Bond, 2011: North Pacific Decadal Variability and Climate Change in the IPCC AR4 Models. *Journal of Climate*, **24 (12)**, 3049–3067, doi:10.1175/2010JCLI3584.1.

Garfinkel, C. I., M. M. Hurwitz, D. W. Waugh, and A. H. Butler, 2013: Are the teleconnections of Central Pacific and Eastern Pacific El Niño distinct in boreal wintertime? *Climate Dynamics*, **41 (7-8)**, 1835–1852, doi:10.1007/s00382-012-1570-2.

Gelaro, R., et al., 2017: The Modern-Era Retrospective Analysis for Research and Applications, Version 2 (MERRA-2). *Journal of Climate*, **30 (14)**, 5419–5454, doi:10.1175/JCLI-D-16-0758.1.

Gent, P. R., et al., 2011: The Community Climate System Model Version 4. *Journal of Climate*, **24 (19)**, 4973–4991, doi:10.1175/2011JCLI4083.1.

Gill, A. E., 1980: Some simple solutions for heat-induced tropical circulation. *Quarterly Journal of the Royal Meteorological Society*, **106 (449)**, 447–462, doi:10.1002/qj.49710644905.

Goddard, L. and M. Dilley, 2005: El Niño: Catastrophe or Opportunity. *Journal of Climate*, **18 (5)**, 651–665, doi:10.1175/JCLI-3277.1.

Hartmann, D. L., 2015: Pacific sea surface temperature and the winter of 2014. *Geophysical Research Letters*, **42 (6)**, 1894–1902, doi:10.1002/2015GL063083.

Hartmann, D. L., H. H. Hendon, and R. A. Houze, 1984: Some Implications of the Mesoscale Circulations in Tropical Cloud Clusters for Large-Scale Dynamics and Climate. *Journal of the Atmospheric Sciences*, **41 (1)**, 113–121, doi:10.1175/1520-0469(1984)041⟨0113:SIOTMC⟩2.0.CO;2.

Horel, J. D. and J. M. Wallace, 1981: Planetary-Scale Atmospheric Phenomena Associated with the Southern Oscillation. *Monthly Weather Review*, **109 (4)**, 813–829, doi:10.1175/1520-0493(1981)109⟨0813:PSAPAW⟩2.0.CO;2.

Hoskins, B. J. and D. J. Karoly, 1981: The Steady Linear Response of a Spherical Atmosphere to Thermal and Orographic Forcing. *Journal of the Atmospheric Sciences*, **38 (6)**, 1179–1196, doi:10.1175/1520-0469(1981)038⟨1179:TSLROA⟩2.0.CO;2.

Iza, M. and N. Calvo, 2015: Role of Stratospheric Sudden Warmings on the response to Central Pacific El Niño. *Geophysical Research Letters*, **42 (7)**, 2482–2489, doi:10.1002/2014GL062935.

Kalnay, E., et al., 1996: The NCEP/NCAR 40-Year Reanalysis Project. *Bulletin of the American Meteorological Society*, **77 (3)**, 437–471, doi:10.1175/1520-0477(1996)077⟨0437:TNYRP⟩2.0.CO;2.

Kim, S. T. and J.-Y. Yu, 2012: The two types of ENSO in CMIP5 models. *Geophysical Research Letters*, **39 (11)**, doi:10.1029/2012GL052006.

Leathers, D. J., B. Yarnal, and M. A. Palecki, 1991: The Pacific/North American Teleconnection Pattern and United States Climate. Part I: Regional Temperature and Precipitation Associations. *Journal of Climate*, **4 (5)**, 517–528, doi:10.1175/1520-0442(1991)004⟨0517:tpatpa⟩2.0.co;2.

Liu, Z. and E. Di Lorenzo, 2018: Mechanisms and Predictability of Pacific Decadal Variability. *Current Climate Change Reports*, **4 (2)**, 128–144, doi:10.1007/s40641-018-0090-5.

Mantua, N. J., S. R. Hare, Y. Zhang, J. M. Wallace, and R. C. Francis, 1997: A Pacific Interdecadal Climate Oscillation with Impacts on Salmon Production. *Bulletin of the American Meteorological Society*, **78 (6)**, 1069–1079, doi:10.1175/1520-0477(1997)078⟨1069:APICOW⟩2.0.CO;2.

McCabe, G. J. and D. M. Wolock, 2008: Joint Variability of Global Runoff and Global Sea Surface Temperatures. *Journal of Hydrometeorology*, **9 (4)**, 816–824, doi:10.1175/2008JHM943.1.

NASA Goddard Institute for Space Studies (NASA/GISS), 2018a: NASA-GISS GISS-E2.1G model output prepared for CMIP6 CMIP piControl. Earth System Grid Federation, doi:10.22033/ESGF/CMIP6.7380.

NASA Goddard Institute for Space Studies (NASA/GISS), 2018b: NASA-GISS GISS-E2.1H model output prepared for CMIP6 CMIP piControl. Earth System Grid Federation, doi:10.22033/ESGF/CMIP6.7381.

Newman, M., G. P. Compo, and M. A. Alexander, 2003: ENSO-Forced Variability of the Pacific Decadal Oscillation. *Journal of Climate*, **16 (23)**, 3853–3857, doi:10.1175/1520-0442(2003)016⟨3853:EVOTPD⟩2.0.CO;2.

Penland, C. and P. D. Sardeshmukh, 1995: The Optimal Growth of Tropical Sea Surface Temperature Anomalies. *Journal of Climate*, **8 (8)**, 1999–2024, doi:10.1175/1520-0442(1995)008⟨1999:TOGOTS⟩2.0.CO;2.

Pierce, D. W., T. P. Barnett, N. Schneider, R. Saravanan, D. Dommenget, and M. Latif, 2001: The role of ocean dynamics in producing decadal climate variability in the North Pacific. *Climate Dynamics*, **18 (1-2)**, 51–70, doi:10.1007/s003820100158.

Rasmusson, E. M. and T. H. Carpenter, 1982: Variations in Tropical Sea Surface Temperature and Surface Wind Fields Associated with the Southern Oscillation/El Niño. *Monthly Weather Review*, **110 (5)**, 354–384, doi:10.1175/1520-0493(1982)110⟨0354:VITSST⟩2.0.CO;2.

Rayner, N. A., D. E. Parker, E. B. Horton, C. K. Folland, L. V. Alexander, D. P. Rowell, E. C. Kent, and A. Kaplan, 2003: Global analyses of sea surface temperature, sea ice, and night marine air temperature since the late nineteenth century. *Journal of Geophysical Research D: Atmospheres*, **108 (14)**, 4407, doi:10.1029/2002jd002670.

Ridley, J., M. Menary, T. Kuhlbrodt, M. Andrews, and T. Andrews, 2018: MOHC HadGEM3-GC31-LL model output prepared for CMIP6 CMIP piControl. Earth System Grid Federation, doi:10.22033/ESGF/CMIP6.6294.

Rodionov, S., N. Bond, and J. Overland, 2007: The Aleutian Low, storm tracks, and winter climate variability in the Bering Sea. *Deep Sea Research Part II: Topical Studies in Oceanography*, **54 (23-26)**, 2560–2577, doi:10.1016/j.dsr2.2007.08.002.

Rogers, J. C., 1981: The North Pacific Oscillation. *Journal of Climatology*, **1 (1)**, 39–57, doi:10.1002/joc.3370010106.

Sardeshmukh, P. D. and B. J. Hoskins, 1988: The Generation of Global Rotational Flow by Steady Idealized Tropical Divergence. *Journal of the Atmospheric Sciences*, **45 (7)**, 1228–1251, doi:10.1175/1520-0469(1988)045⟨1228:TGOGRF⟩2.0.CO;2.

Schneider, N. and B. D. Cornuelle, 2005: The Forcing of the Pacific Decadal Oscillation*. *Journal of Climate*, **18 (21)**, 4355–4373, doi:10.1175/JCLI3527.1.

Schoennagel, T., T. T. Veblen, W. H. Romme, J. S. Sibold, and E. R. Cook, 2005: ENSO and PDO variability affect drought-induced fire occurrence in rocky mountain subalpine forests. *Ecological Applications*, **15 (6)**, 2000–2014, doi: 10.1890/04-1579.

Seviour, W. J. M., L. J. Gray, and D. M. Mitchell, 2016: Stratospheric polar vortex splits and displacements in the high-top CMIP5 climate models. *Journal of Geophysical Research: Atmospheres*, **121 (4)**, 1400–1413, doi:10.1002/2015JD024178.

Shi, J., A. V. Fedorov, and S. Hu, 2019: North Pacific temperature and precipitation response to El Niño-like equatorial heating: sensitivity to forcing location. *Climate Dynamics*, **53 (5-6)**, 2731–2741, doi:10.1007/s00382-019-04655-x.

Siler, N., Y. Kosaka, S. P. Xie, and X. Li, 2017: Tropical Ocean Contributions to California's Surprisingly Dry El Niño of 2015/16. *Journal of Climate*, **30 (24)**, 10 067–10 079, doi:10.1175/JCLI-D-17-0177.1.

Smith, D. M., et al., 2019: Robust skill of decadal climate predictions. *npj Climate and Atmospheric Science*, **2 (1)**, 13, doi:10.1038/s41612-019-0071-y.

Sun, T. and Y. M. Okumura, 2019: Role of Stochastic Atmospheric Forcing from the South and North Pacific in Tropical Pacific Decadal Variability. *Journal of Climate*, **32 (13)**, 4013–4038, doi:10.1175/JCLI-D-18-0536.1.

Swart, N. C., et al., 2019: CCCma CanESM5 model output prepared for CMIP6 CMIP piControl. Earth System Grid Federation, doi:10.22033/ESGF/CMIP6.3673.

Tang, Y., S. Rumbold, R. Ellis, D. Kelley, J. Mulcahy, A. Sellar, J. Walton, and C. Jones, 2019: MOHC UKESM1.0-LL model output prepared for CMIP6 CMIP piControl. Earth System Grid Federation, doi:10.22033/ESGF/CMIP6.6298.

Tatebe, H. and M. Watanabe, 2018: MIROC MIROC6 model output prepared for CMIP6 CMIP piControl. Earth System Grid Federation, doi:10.22033/ESGF/CMIP6.5711.

Taylor, K. E., R. J. Stouffer, and G. A. Meehl, 2012: An overview of CMIP5 and the experiment design. *Bulletin of the American Meteorological Society*, **93 (4)**, 485–498, doi:10.1175/BAMS-D-11-00094.1.

Tompkins, A. M., 2001: On the Relationship between Tropical Convection and Sea Surface Temperature. *Journal of Climate*, **14 (5)**, 633–637, doi:10.1175/ 1520-0442(2001)014⟨0633:OTRBTC⟩2.0.CO;2.

van Loon, H. and K. Labitzke, 2011: *Interannual Variations in the Stratosphere of the Northern Hemisphere: A Description of Some Probable Influences.* Geophysical Monograph Series, American Geophysical Union (AGU), 111–122 pp., doi:10.1029/ gm075p0111.

Vimont, D. J., D. S. Battisti, and A. C. Hirst, 2001: Footprinting: A seasonal connection between the tropics and mid-latitudes. *Geophysical Research Letters*, **28 (20)**, 3923–3926, doi:10.1029/2001GL013435.

Vimont, D. J., J. M. Wallace, and D. S. Battisti, 2003: The Seasonal Footprinting Mechanism in the Pacific: Implications for ENSO. *Journal of Climate*, **16 (16)**, 2668–2675, doi:10.1175/1520-0442(2003)016⟨2668:TSFMIT⟩2.0.CO;2.

Wallace, J. M. and D. S. Gutzler, 1981: Teleconnections in the Geopotential Height Field during the Northern Hemisphere Winter. *Monthly Weather Review*, **109 (4)**, 784–812, doi:10.1175/1520-0493(1981)109⟨0784:TITGHF⟩2.0.CO;2.

Wang, C., 2018: A review of enso theories. *National Science Review*, **5 (6)**, 813–825, doi:10.1093/nsr/nwy104.

Wills, R. C., D. S. Battisti, C. Proistosescu, L. A. Thompson, D. L. Hartmann, and K. C. Armour, 2019: Ocean Circulation Signatures of North Pacific Decadal Variability. *Geophysical Research Letters*, **46 (3)**, 1690–1701, doi:10.1029/2018GL080716.

Wu, T., et al., 2018: BCC BCC-CSM2MR model output prepared for CMIP6 CMIP piControl. Earth System Grid Federation, doi:10.22033/ESGF/CMIP6.3016.

Yeh, S. W., J. S. Kug, B. Dewitte, M. H. Kwon, B. P. Kirtman, and F. F. Jin, 2009: El Niño in a changing climate. *Nature*, **461**, 511–514, doi:10.1038/nature08316.

Yu, J. Y. and S. T. Kim, 2011: Relationships between Extratropical Sea Level Pressure Variations and the Central Pacific and Eastern Pacific Types of ENSO. *Journal of Climate*, **24 (3)**, 708–720, doi:10.1175/2010JCLI3688.1.

Zhang, C., 2005: Madden-julian oscillation. *Review of Geophysics*, **43 (2)**, 1–36, doi:10.1029/2004RG000158.

Zhang, J., et al., 2018a: BCC BCC-ESM1 model output prepared for CMIP6 CMIP piControl. Earth System Grid Federation, doi:10.22033/ESGF/CMIP6.3017.

Zhang, Y., S. P. Xie, Y. Kosaka, and J. C. Yang, 2018b: Pacific Decadal Oscillation: Tropical Pacific Forcing versus Internal Variability. *Journal of Climate*, **31 (20)**, 8265–8279, doi:10.1175/JCLI-D-18-0164.1.